Mississippi State University

Scholars Junction

5-1-2014

A Multi-Decadal Remote Sensing Study on Glacial Change in the North Patagonia Ice Field Chile

Lucy Korlekwor Tetteh

Follow this and additional works at: https://scholarsjunction.msstate.edu/td

A multi-decadal remote sensing study on glacial change in the North Patagonia Ice field

Chile

By

Lucy Korlekwor Tetteh

A Thesis
Submitted to the Faculty of
Mississippi State University
in Partial Fulfillment of the Requirements
for the Degree of Master of Science
in Geosciences
in the Department of Geosciences

Mississippi State, Mississippi

May 2014

A multi-decadal remote sensing study on glacial change in the North Patagonia Ice field

Chile

By

Lucy Korlekwor Tetteh

Approved:

_____
Shrinidhi S. Ambinakudige
(Major Professor)

_____
Qingmin Meng
(Committee Member)

_____
Padmanava Dash
(Committee Member)

_____
Michael E. Brown
(Graduate Coordinator)

_____
R. Gregory Dunaway
Dean
College of Arts & Sciences

Name: Lucy Korlekwor Tetteh

Date of Degree: May 17, 2014

Institution: Mississippi State University

Major Field: Geosciences

Major Professor: Shrinidhi Ambinakudige

Title of Study: A multi-decadal remote sensing study on glacial change in the North Patagonia Ice field Chile

Pages in Study: 91

Candidate for Degree of Master of Science

Glaciers in the North Patagonian Ice Fields are temperate glaciers and can be studied to understand the dynamics of climate change. However, the ice field has been neglected in mass balance studies. In this study, multi decadal study of glacial mass balance, glacier retreat and glacial lake expansion in the North Patagonia were studied. Landsat (TM, ETM+ and 8) and ASTER images were used. San Quintin glacier experienced the highest retreat. Demarcation of glacier lakes boundaries indicated an increase in glacial lake area from 13.49 km^2 to 65.06 km^2 between 1979 and 2013, with an addition of 4 new glacial lakes. Nef glacier recorded the highest mass gain of 9.91±1.96 m.w.e.a.$^{-1}$ and HPN-4 glacier recorded the highest mass loss of -8.9±1.96 m.w.e.a.$^{-1}$. However, there is a high uncertainty in the elevation values in the DEM due to the rugged nature of the terrain and presence of the heavy snow cover.

Key Words: Mass balance, Glacier, ASTER, DEM, North Patagonia, Chile

DEDICATION

This thesis is dedicated to the Almighty God for providing me with such a great opportunity. Secondly, to my loving family members who have offered their encouragement and support throughout my graduate study. Special thanks to my father, John Eric Tetteh; mother, Juliana Anastasia Tetteh, brothers, Henry Tetteh and Harry Tetteh and sister, Felicity Tetteh.

ACKNOWLEDGEMENTS

TABLE OF CONTENTS

LIST OF TABLES

LIST OF FIGURES

CHAPTER I

INTRODUCTION

Chapter one provides an introduction of various topics on glaciers and climate change within the North Patagonia Ice Field (NPI). Section 1.1 provides background information on glacier formation. Section 1.2 gives general information on glacier mass balance measurement techniques. The reason why this study is very important is stated in the problem statement in Section 1.3. This study's objectives are listed in Section 1.4 and hypothesis in Section 1.5. Section 1.6 describes the geographic setting and climatic conditions governing the study area. Section 1.8 provides the research scope and the study's limitations. Section1.9 gives the thesis organization which is a synopsis of the individual chapters.

Background

Glacier is defined as the slow movement of ice and snow under its own weight, which is formed when the accumulation of snow exceeds ablation (Ambinakudige, 2014). While snowfall, wind drift, avalanches, freezing rain, and meltwater cause accumulation, ablation is caused by melting, sublimation, wind erosion, loss of ice by avalanche, or calving of icebergs (Ambinakudige, 2014, Braithwaite, 2002). Glacier gains mass when snow accumulates, and looses mass when snow melts. Glaciers are key indicators for assessing climate change (Ambinakudige, 2010, Bolch et al., 2008, IPCC, 2013).

1

Beginning 19th century, glaciers in many parts of the world have retreated due to global climate change (Liu et al., 2005). The NPI and South Patagonian Ice Field have the largest temperate ice mass in the southern hemisphere (Warren and Sugden, 1993). These temperate glaciers always have their temperature at melting point. Therefore, global reduction in these snow-covered areas is the clearest indicators of climate warming (IPCC, 2007). Understanding the current state is very key to make future predictions of their evolution (Casassa et al., 2007). The retreat and reduction in glacier mass is very evident in the past decade in Patagonia of Chile (Aniya, 1999; Rignot et al., 2003; Rivera et al., 2007; Casassa et al., 2007; Lopez et al., 2010). The main consequences are the uncertainty on how much the glacier melt in this region contributes to sea level rise (Rignot and Casassa, 2003), the long term decrease in water runoff, and the increase in Glacier Outburst Floods (GLOF) events (Casassa et al., 2010). Most of the studies in the North Patagonia Ice Field (NPI) concentrate on ice thinning rates. Only a hand-full have tried to estimate mass balance for this region. This is due to the inaccessibility and difficulty to perform field work and lack of high resolution satellite images for this region. An accurate estimation of mass balance of mountain glaciers, such as the NPI, would help to understand the impacts of climate change to sea level rise and glacial lakes formation, and develop an early warning system in the case of Glacier Lake Outburst Floods, which causes disaster in the vulnerable downstream localities. Glacier Lake Outburst Floods is a disastrous discharge of large volume of water due to the breaking of the moraine dammed lakes (Yamanda and Sharma, 1993). Glacier lakes form due to melting of glacier ice and snow. High melting rates have increased the threat of glacial lake outburst in high mountain range of the world (Huggel et. al., 2002). Various natural

phenomenon such as avalanche, earth quake or even the weight of water itself breaking the moraine dams lead to GLOF. There are several GLOF events in Andean glacial regions. An example is the late 2000 GLOF in the North Patagonia Ice field, where a rock fall partially displaced Lake Lago Calafate and caused an outburst (Harrison et. al., 2006).

Glacier mass balance measurement

Glacier mass balance study is the study of the changes that occur to a glacier from year to year (Paterson, 1994). A positive mass balance is achieved when accumulation exceeds ablation in a particular year, while negative mass balance occurs when the ablation exceeds accumulation (Braithwaite, 2002). There are direct and indirect methods of mass balance measurement. The direct method, which involves an *in-situ* collection of glacier data, has been in use since the 1940s to measure retreats and mass balance usually conducted at lower ablation regions (Rott et al., 2002; Nishida et al., 1995). Due to the inaccessibility of most glaciated areas around the world, direct methods are being used less frequently, and studies using indirect methods have become common in glacier studies (Barry, 2006; Dyurgerov and Meier, 1997). Indirect method of mass balance measurement requires the use of remote sensing techniques, which involves use of satellite images, aerial photos, and photogrammetric methods (Racoviteanu et al., 2008; Ambinakudige and Joshi, 2013). Since this method is indirect, it helps to eliminate the hectic field visits, and also grants access to inaccessible areas.

Another factor that can cause a glacier to lose mass is glacier retreat. Globally, the most important factor that affects glacier retreat but has not been confirmed for tropical glaciers is air temperature (Houghton et al., 2001).

3

Glacier retreat and expansion of glacial lakes

Glacier retreat is the decrease in the area of a glacier by the breaking off or melting of areas along the glacier tongue and boundaries. The retreat of glaciers indicates climate change (Ambinakudige, 2010). Satellite images that are commonly used to study glacier retreat (Ambinakudige, 2010; Lopez et al., 2010; Howat and Eddy, 2011; López-Moreno et al., 2014) and expansion of glacial lakes, (Bolch et al., 2012; Wu et al., 2012; Loriaux and Casassa, 2013) are Landsat, ASTER, SPOT and many other satellite images.

There are two ways to measure glacier retreat and glacial lake expansion. The glacier tongue positions for the years in study can be digitized on the satellite image. The retreat is then measured by the change in position of the glacier tongue during the study period (Lopez et al., 2010; Howat and Eddy, 2011; López-Moreno et al., 2014). Similarly, glacial lakes can be digitized using visual interpretation of satellite images for the different years in study region and then glacial lake area can be calculated (Wu et al., 2012; Loriaux and Casassa, 2013).

The second way to measure glacier retreat and glacial lakes is to employ the Normalized Difference Water Index (NDWI) for lake detection. This method is used where glacial lakes are found at the tongue of glaciers. Various image ratios and band combinations have been used to delineate the glacier tongue locations (Huggel et al., 2002; Ambinakudige, 2010; Hoffmann and Weggenmann, 2013). Based on the NDWI, the difference in glacial lake areas and distance in retreat can be computed.

Problem statement

The NPI and Southern Patagonia Ice field (SPI) together have the largest temperate ice mass in the southern hemisphere (Warren and Sugden, 1993). Temperate

glaciers are glaciers that have their temperatures always at melting point throughout the glacier (Aniya et al., 1996). These types of glaciers respond to climate changes in a short period (Aniya et al., 1996). Therefore such glaciers need to be studied in order to understand the dynamics of climate change. Also, the dataset/inventory of the World Glacier Monitoring Service (WGMS, 1991) is populated with inventory of European, North American and glaciers in the northern hemisphere. Glacier inventory of the Patagonian glaciers are lacking in the WGMS dataset. The Patagonia glaciers have been neglected for mass balance studies even though other important works have been undertaken in the area (Warren and Sugden, 1993).

Schaefer et al., (2013) modeled the surface mass balance of the NPI. This is the only recorded studies on mass balance that considered the entire glacier in this region. Studies on the thinning rates of glaciers in the NPI have been performed (Aniya, 1988; Aniya, 1996; Aniya, 1999; Rignot et al., 2003; Rivera et al., 2007). Lopez et al. (2008) monitored the snow cover in the NPI. Pellicciotti et al. (2013) studied the changes of glaciers in the Andes of Chile using an advanced mass balance model. Glacial lakes have also been measured (Loriaux and Casassa, 2012).

Aniya et al., (1996) states four reasons for which the mass balance studies is lacking in this area: 1) this area is rarely inhabited by local residents, therefore the glacier conditions will not influence the local people, 2) the ice field is located far from Europe and North America and thus neglected by the European researchers, 3) local scientists show less interest. And lastly, due to the remoteness, inaccessibility and bad weather condition associated with the ice fields, it is difficult to perform field mass balance studies in the NPI

Due to the sparse mass balance research, there is a big gap in the NPI mass balance records. Considering the facts that there is less glacier inventory in this region, uncertainty on how these glacier melt contribute to sea level rise (Rignot and Casassa, 2003) and the fact that most water resources are obtained from glacier melt, more glacier studies need to be performed to gain records on water balances and annual mean discharges in this region (Escober et al., 1992). This study analyzes the spatial and temporal mass balance of the NPI, glacial retreat and expansion of glacial lake in this area using remote sensing methods. Study results will make significant contributions to the mass balance inventory of the Patagonia Ice field in Chile.

Study objectives

The specific objectives of this study were:

1. To estimate mass balance of major glaciers in North Patagonia Ice Field between 2007 and 2012 using remote sensing techniques.

2. To measure the multi-decadal retreat of the North Patagonian glaciers and

3. To analyze the expansion of glacial lakes using topographic maps and Landsat (TM, ETM+ and 8) images between 1979 and 2013.

4. Hypothesis

The Null hypotheses that were tested in this study were :

1. There was no significant mass change in glaciers in the North Patagonia Ice Field from 2007 to 2012.

2. There is no significant retreat in the glacier tongues and

3. The number and area of glacial lakes remained the same from 1979 to 2013.

Study area: North Patagonian Ice Field
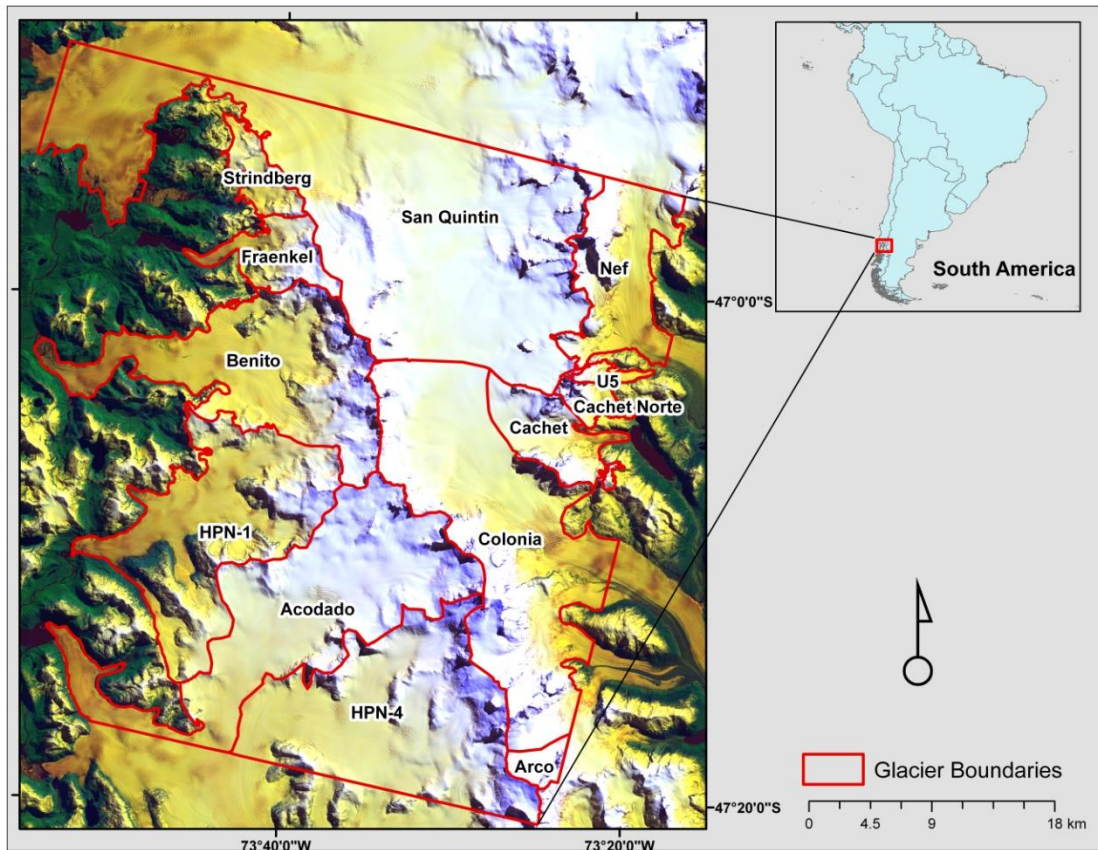
Figure 1.1   Glaciers in the North Patagonia Ice Fields

Source: Digitized from Landsat 8 satellite image (Band 5, Band 3 and Band 1).

The NPI is located between 46°30'S and 47°30'S, along 73°30′W and it stretches for approximately 100 km along 73°30'W, covering a total area of 4200 km^2 (Aniya, 1988). It has a width of approximately 71 km in the west-east direction from the tongues of San Quintin glacier to Soler glacier (Lopez et al., 2010). Majority of the glaciers lies in altitudes of 1000 m on the west and 1500 m on the east. San Valentin summit (3910 m above sea level) is the highest point on the NPI (Lopez and Casassa, 2011), which is

located on the north-eastern part of the ice field. The lowest altitude is the sea level located on the Laguna San Rafael located at the western side of the NPI near the Pacific Ocean. A northwest to southeast line of nunataks divides the northeast ice field from the southwest ice field. This forms the accumulation area for the Colonia glacier (Warren and Sugden, 1993). Twenty eight outlet glaciers are present in the NPI (Warren and Sugden, 1993), but for this study, 13 glaciers are considered. San Quintin glacier and San Rafael glaciers are the largest glaciers in the NPI, each with an area of about 760 km^2, followed by Steffan and Colonial glaciers (Aniya, 1988). San Rafael is the only tidewater calving glacier in the NPI. Most of the other glaciers have freshwater calving fronts (Rivera et. al., 2007). Both calving glacier types respond directly to climate change (Warren and Aniya, 1999).

Equilibrium Lines of Altitude (ELA) is an area on a glacier that separates the accumulation zone from the ablation zone (Braithwaite, 2010). An ELA of about 900 to 1350 m separates the NPI into 2578 km^2 of accumulation zone and a 1550 km^2 of ablation zone (Aniya, 1988). Due to the climatic conditions, topography and the nunataks that divides the ice field, the western outlet glaciers are larger and more active than the eastern glaciers (Aniya and Enomoto, 1986; Lopez et al., 2010).

San Rafael glacier has the largest accumulation zone, followed by San Quintin glacier and then Steffen and Colonia glaciers (Aniya, 1988). San Quintin glacier on the other hand has the largest ablation area of about 26% of the ablation are on the ice field. This is followed by San Rafael, Steffan and Colonia glaciers respectively (Aniya, 1988).

Over the last 60 years, Aniya (2007) indicated a general retreat of 21 glaciers in the NPI. After the 1990s, he observed an increase in the rates of retreats, with the western side experiencing more retreat than on the eastern side (Aniya, 1992).

The NPI is in the Wet Andes region (Lliboutry, 1998). The NPI receives abundant precipitation of about 2000 to 11000 mm of water equivalent per year (Rignot and Casassa, 2003). The east side on the other hand has annual precipitation of approximately 1500 mm (Enomoto and Nakajima, 1985).This precipitation is predominantly attributed to the mid-latitudes storms that moves westward between 40°S and 50°S, as well as the mean latitudinal locations of the storm tracks which is closely related to the axis of the westerly winds in middle and upper troposphere (Gerreaud et al., 2007).

The westerly winds become very strong and near permanent when the mean air temperature at sea level decreases gradually from 13.7°C at latitude 37°23' South to 6.5°C at latitude 53°10' South (Lliboutry, 1998). The NPI is also characterized by the Föhn winds, which are dry, warm, and down-slope winds. These winds lead to dry conditions and high temperatures on the eastern side of the ice field. They also increase the precipitation gradient in the west - east direction (Fujiyoshi et al., 1987). But the precipitation in the NPI shows no significant seasonality (Carrasco et al., 2002).The elevation of the limit between rainfall and snowfall during precipitation events is the main climatic factor causing glacier fluctuations in the NPI (Lliboutry, 1998).

Research scope and limitations

Ground-truth data is non-existent to validate this study except the comparison with studies performed by Aniya (1988), Aniya (1999), Aniya et al., (1996) and Rignot et al., (2003) for glacier thinning studies and Lopez et al., (2010), Loriaux and Casassa

(2012) and Rivera et al., (2007) for glacier retreat and lakes. This thesis estimates mass balance of 13 glaciers in NPI area using remote sensing methods, measures the glacier retreat of 9 glaciers and the expansion of 9 glacier lakes.

Uncertainty in this study is due to the low quality of the DEMs generated, which is because of the rugged terrain associated with the NPI and the high vertical random error of 17 m (Falkner, 1995) of the topographic map. The unavailability of *in-situ* data from the study area and the lack of Ground Control Points (GCPs) from the field to georeference satellite images will affect the creation of high accuracy DEMs.

Thesis organization

Chapter 1 (Introduction) provides a general summary of the background of the research, study objectives and hypothesis, a brief introduction of study area and its climatic setting, study limitations, and the significance of this study to the scientific community. Chapter 2 (Literature Review) reviews previous glacier studies and data gaps of mass balance studies in the NPI. Chapter 3 (Research Methods) describes the methods and computations involved in fulfilling the objectives of this study. Chapter 4 (Results and Discussion) provides the glacier mass balance estimation, glacier retreat and expansion of glacial lake results of the glaciers considered in this study, in comparison to previous studies. Chapter 5 (Conclusions and Recommendations) summarizes the entire results in the study, challenges, and suggestions for further research.

CHAPTER II

LITERATURE REVIEW

This chapter provides insight of previous mass balance, glacier retreat and glacial lake expansion studies, and the method and data used. A section is provided on the North Patagonia Ice Field to discuss the glacier studies in this region.

Mass Balance Measurement of Glaciers

Mass balance measurements and analysis of glaciers can be performed in two major ways. That is either by direct measurements or indirect measurements. Direct measurements involve *in-situ* collection of glacier data, where a visit to the study site is performed to record measurement. Indirect measurements involve employing remote sensing techniques of data analysis. Due to the inaccessibility of most glacier locations, the direct method is impossible in certain cases and more studies are based on indirect methods (Barry, 2006; Dyurgerov and Meier, 1997).

Direct/*in-situ* method

This involves direct interactions with the glacier on the study area. This method is very stressful and labor intensive, since it involves digging to measure the elevation of ice at different time, depth and location. This method is known as the glaciological method, and was first employed at the end of the 19th century in Europe's Rhone glacier (Dyurgerov and Meier, 2000; Zemp et al., 2009). Ablation stakes are buried in the ice so

that accumulation and ablation of snow can be measured with the stake as a reference point at a later time (La Frenierre, 2009; Zemp et al., 2009; Fischer, 2011). The change in volume of the glacier can be computed by finding the product of the glacier area and the change in depth/height of the glacier at any given time period (Kaser et al., 2003). The mass balance can then be calculated by multiplying the volume by the density of ice (900 kgm^{-3}).

Another direct method of mass balance measurement is the geodetic survey method. A geodetic survey using the Global Positioning System (GPS) (Kaser et al., 2003) or a total station (Schaffhauser et al. 2008) can be performed from a stable place (e.g. non-glaciated), to measure the x, y, z of the location. The same measurements can be performed at a different time period at the exact location. The difference in elevation can then be computed, multiplied by the glacier area and ice density to achieve the mass balance (Hubbard and Glasser, 2005).

Direct mass balance measurements can also be performed using the climate models. With this method, non-climatic influences on mass balance such at kinematic waves, avalanches and surges needs to be excluded. Glacier models are then generated from the accurate and available climate data. But to begin with, there should be at least some mass balance data in order to generate the model. Majority of the models are built based on simple precipitation data since data on precipitation distribution and accumulation are complex. And all the models should be calibrated for each individual glacier (Kaser et al., 2003). Another climate model method is by using temperature-index models and an accumulation model (Huss and Bauder, 2009). These temperature-index models operate on linear relationship between melt rate and positive air temperature

13

(Huss and Bauder, 2009). Daily temperature and precipitation are used as inputs for the models. Daily precipitation sums is multiplied by a correction factor to obtain the accumulation and ablations (Huss and Bauder, 2009).

Indirect/remote sensing method

This method involves the use of digital or satellite images in mass balance calculations. This is cost effective and eliminates the labor involved in field measurements. The change in elevation of an area between two different time periods are obtained from stereoscopic satellite images such as ASTER, SRTM, ALOS/PRISM or SPOT5 (Racoviteanu et al., 2008; Lopez et al., 2010; Bolch et al., 2011). This means that satellite images used for glacier measurements should have the capabilities of generating Digital Elevation Models (DEMs). This elevation by pixel is multiplied by the glacier area to obtain the volume. The volume is then multiplied by the density of ice to obtain the mass balance (Paterson, 1994).

The readily availability of satellite images and topographic maps makes this method of mass balance measurement to be highly adopted in most studies. Examples of such research are DEMs generated from ASTER (Casey et al., 2012), SRTM (Racoviteanu et al., 2008) and SPOT imagery (Berthier et al., 2007).

Bolch et al., (2011) used 1970 Corona KH-4b, 1984 aerial photographs, 2007 Cartosat-1 images and Digital Terrain Models (DTMs) for 1962 Corona and 2002 ASTER to study the multi-decadal mass loss of glaciers in the Everest area in the Himalayas. With 14 non-differential GPS points and approximately 200 points extracted from a 1:50,000 topographic map, DTMs were generated for the area. Relative uncertainties in the DTM were calculated based on non-glaciated area. The change in

volume of the glaciers were calculated assuming a stable density profile. The volume change is then multiplied by the density of ice (900 kg m^{-3}) to convert it to mass change.

Ambinakudige and Joshi, (2013) estimated the mass balance of Fedchenko Glacier, Tajikistan between 2004 and 2009 using ASTER satellite images. Relative DEMs of the Fedchenko and its neighboring glaciers were generated from the ASTER satellite images for 2004 and 2009. About a thousand random points were used to extract the elevation values from the DEMS. The mean elevation difference between the two images was multiplied by the glacier area, which was then multiplied by the density of ice to estimate the specific mass balance.

Pieczonka et al., (2013) studied the heterogeneous mass loss of glaciers in the Aksu-Tarim Catchment (Central Tien Shan) by using a 1976 KH-9 Hexagon and 2009 SPOT-5 satellite images. Thirty eight GCPs were extracted from a topographic map and DTMs were generated from the SPOT-5 image and the KH-9 Hexagon image using the PCI Geomatics software and the Lieca Photogrammety Suite respectively. Mass balance is then calculated by multiplying the mean elevation differences between the two time periods by the density of ice. They further converted the mass balance to m.w.e.a^{-1} by multiplying by 999.972 kgm^{-3}.

Digital elevation model creation and accuracy

A Digital Elevation Model (DEM) is a digital 3D representation of the earth's surface. Mass balance values obtained from DEM calculation are commonly used when the study is located in an inaccessible area (Bolch et al., 2011; Nuth and Kaab, 2011). This is because the difference in elevation values between different time periods can be either be positive or negative, which corresponds to accumulation and ablation

15

respectively. Elevation differences can also show no change in elevation values. As such, satellite images that are used in mass balance studies have the capabilities of capturing stereoscopic images to generate DEMs (Ambinakudige and Joshi, 2013). The generation of quality DEM over a large area is a challenging and a complicated process. As such, open source DEMs such as SRTM, ASTER Global DEM, GTOPO 30 are normally used as reference DEMs even though they are of coarser resolution (Mukherjee et al., 2013). The most common satellites used in DEM creation are ASTER, ALOS, SRTM, SPOT 5 and CORONA KH-4, KH 4A and KH 4B (Ambinakudige and Joshi, 2013). The across-track incidence angles that are opposite to each other produce a base-to-height ratio (B/H) of 0.61, which favors the generation of DEM in high mountainous areas (Berthier et al., 2007). SPOT satellites (1 - 4) has so far proven to be the most successful in DEM creation with automated stereocorrelation accuracy between ±5 and ±20 m root-mean-square error (RMSE) in the Z-coordinates (Hirano et al., 2003). However, the SPOT (1 - 4) are very costly and it is very difficult to obtain cloud-free images covering a lot of areas in the world (Hirano et al., 2003).

Hirano et al., (2003) examined the accuracy of ASTER DEMs on four locations including the Andes Mountains, Chile-Bolivia in South America. The Andes Mountains study area has the Pampa Luxsar lava complex with elevation ranges from relatively low, flat lava flow areas to high cone-shaped volcanoes with approximately 5700 m in elevation. With an ASTER stereopair (Level 1A) image, a DEM was generated with 18 GCPs and 53 check points. Validating DEM with a 1:50,000 scale topographic map yielded an RMSE of ±15.8 m in the Z-coordinates. It is expected that the evaluation of the vertical accuracy of ASTER images produces an RMSE of ±7 to ±20 m (Hirano et al.,

16

2003). Therefore, the RMSE achieved by using ASTER images for DEM creation of the Andes Mountains falls between the expected ranges.

Berthier et al., (2007) estimated the glacier mass balances in Himachal Pradesh (Western Himalaya, India) by comparing a 2004 DEM derived from two SPOT 5 satellite images to the 2000 SRTM DEM. The DEM from the SPOT 5 was generated without any GCPs. This could be achieved due to the good on-board geolocation of SPOT 5 scenes. The SRTM DEM was used as a reference DEM in the SPOT 5 DEM generation. Due to the absence of topographic maps for GCPs extraction, about a hundred automatic GCPs were generated from the SPOT 5 images, due to the accurate geolocation of the images and the presence of SRTM DEM as reference data. They generated the DEM of the SPOT 5 using the PCI Geomatics software. With an accuracy of ±25 m at a 66% confidence interval, each pixel in the SPOT 5 image could be located on the ground. The GCPs had a vertical accuracy of ±18 m in high mountainous areas and a planimetric accuracy of ±25 m. The RMSE in the GCPs were 2.1 m for one SPOT 5 image (November 12th) and 1.7 m for the second SPOT 5 image (November 13th).

Cook et al., (2012) created a new 100 m DEM for the Antarctic Peninsula (63– 70° S) derived from the ASTER Global DEM (AGDEM). The purpose is to minimize the large errors on ice-covered terrain. To do this, they smooth out the erroneous region in the AGDEM by converting the AGDEM to contours and then removing the erroneous contours. They did this based on the idea that high-artefact areas have real surface slope less than approximately 20°. Therefore, few contours are needed to create a new surface topography. The new DEM was validated using ICESat-derived elevations. They then performed an accuracy assessment on the new DEM using GPS positions in SPOT 5

DEMs and Landsat Image Mosaic Antarctica (LIMA) imagery. The new DEM created had a mean elevation difference value of -4 m (± 25 m RMSE) from the ICESat image, whereas the original AGDEM has a -13 m ± 97 m RMSE.

Mukherjee et al., (2013) evaluated the vertical accuracy of open source DEMs from ASTER and SRTM using Cartosat DEM and Survey of India (SOI) height information data on the western part of Siwalik Himalaya. The Cartosat DEM was generated by the orientation of stereo pair. Thirty one well distributed GCPs were collected over the study area with the Leica GPS. By using 15 GCPs as control points and 5 GCPs as check points, the stereo model was oriented and a DEM of 10 m grid size was generated. Elevation values were taken directly from the SOI topographic maps and compared directly with the elevation values of the other DEMs. Eleven GCPs from the SOI topographic maps were used to access the accuracy of the Cartosat DEM. Thirty GCPs from the SOI topographic maps and the 10 m grid spacing Cartosat DEM were used to access the accuracy of the ASTER and SRTM DEM surfaces by making a comparison between the ASTER and SRTM DEM with the GCPs and Cartosat DEM. They noted that the characteristics or nature of the terrain affects the quality and accuracy of the DEM produced. The vertical accuracy shown an RMSE of 12.62 and 17.76 for the ASTER and SRTM DEMs respectively when validated with the Cartosat DEM and SOI topographic maps.

Majority of DEM extraction with stereoscopic satellite images requires a topographic map for GCPs extraction as well as for accuracy assessment, even though there are open source DEMs that can act as reference. The only satellite image that automatic GCP extraction has proved to be successful with less RMSE is the SPOT 5

satellite imagery. But the difficulty associated with acquiring a cloud-free SPOT 5 imagery and the cost involved with the purchase makes it less frequently used. As such, most glacier mass balance studies generate DEMs from ASTER satellite images due to the less cost associated with it and the medium spatial resolution that it comes with.

Glacier studies in the NPI

The glacier inventory of Chilean glaciers, especially the NPI is lacking and incomplete in the WGMS dataset. There are limited ice-thickness data and very few glacier studies have been conducted in the NPI in comparison to other glacier studies all over the world (Rivera et al., 2000). There is only a single mass-balance record for the glaciers of the entire NPI (Pellicciotti et al., 2013). There is also a mass balance record for the Glaciar Echaurren Norte (Rivera et al., 2000) and one firn core (Yamada, 1987) record for San Rafael glacier on the western side of the NPI. The only mass balance studies performed for the entire NPI is Schaefer et al., (2013). They used a combined modeling approach to estimate the mass balance, which will be discussed in detail in the sub-section. Yamada (1987) provided annual estimates on the net balance in 1984/85 for the San Rafael as 3.4 m.w.e.a^{-1}. Matsuoka and Naruse (1999) stated that it is difficult to run mass balance analysis on the whole ice field with the current knowledge because the sensitivity of the snowline to temperature and precipitation varies in term of latitude. They recommend firn core drilling as the way to obtain good and sufficient information to estimate mass balance values.

Glacier thinning studies in the NPI

Rignot et al. (2003) measured the total volume loss in ice in the Patagonian Ice fields by generating DEMs from the 2000 Shuttle Radar Topography Mission (SRTM) and comparing them to DEMs generated from Chile topographic maps earlier aerial cartographic maps for the period of 1968/1975-2000. They found that the 24 glaciers in the NPI are thinning at a rate of 2.63 ± 0.4 km^3 yr^{-1} over a 3481 km^2 area with frontal loss of 0.20 km^3 yr^{-1}. They stated that this accounts for a total volume loss of 3.2 ± 0.4 km^3 yr^{-1} over the total ice field size of 4200 km^2 (Aniya et al., 1996). They suggested that the thinning in the Patagonian glaciers must be due to a negative mass balance influenced by climate change. They stated that majority of the glacier outlets in the NPI are calving glaciers, which respond rapidly to climate change than non-calving glaciers.

Rivera et al. (2007) measured the thinning rates of glaciers in the NPI between 1979 and 2001, by generating DEMs with topographic maps and ASTER satellite images. Thirty five Ground Control Points (GCPs) and 80 Tie Points (TPs) were used in the DEM generation with PCI Geomatics software. They recorded a decrease in glacier area of 3.4 $\pm$ 1.5% (140 ± 61 km^2 of ice) with reference to the total glacier area of the NPI in 1979, which they calculated from a Landsat MSS satellite image. All the glaciers experienced thinning. About 62% of the area loss was observed in the glaciers on the western side of the NPI, with San Quintin glacier experiencing the maximum loss of 33 km^2. HPN 1 glacier experienced thinning rates of -4.00 ± 0.97 myr^{-1}, while Acodado glacier experienced thinning rates of -2.10 ± 0.97 myr^{-1}. On the eastern side of the NPI, Nef glacier recorded the maximum loss of 7.9m representing a 5.7% loss in area with respect to the 1979 area. They also reported that not all the glaciers showed similar pattern in

retreat between 1979 and 2001. Rivera et al., (2007) agrees with Aniya, (1999) about the advances in some glaciers after 1991.There were advances in San Quintin between 1991 and 1994. Colonia and San Rafael also experienced advances between 1996 and 1999. But San Rafael glacier experienced rapid retreats between 1974 and 1992 before it started to advance in 1996.

Lopez and Casassa, (2011) studied the acceleration of ice loss rate in the NPI by comparing three DEMs. The DEMs were the year 2000 SRTM DEM, 2005 SPOT 5 DEM, and a DEM generated based on 1975 topographic maps. They also studied the surface area evolution and glacier length fluctuations of 25 glaciers in the NPI between 2001 and 2011, using Landsat ETM+ satellite images. The measurements of a March 2001 Landsat ETM+ satellite image was compared to a February 2011 Landsat ETM+ satellite image. The 1975 DEM was generated based on a 50,000 scale contour lines, with a 50 m spatial resolution. The SPOT 5 DEM was generated by the High Resolution Sensor (HRS) onboard SPOT 5 satellite. They indicated that majority of the glaciers in the NPI thinned, retreated and lost surface between 1975 to 2005. Few glaciers located on the eastern side, including Nef glacier recorded stability, while majority of the western glaciers suffered stronger wasting. HPN 1 experienced the maximum thinning of 4.4 m yr-1 (3.2% loss relative to the surface area of 2001), followed by Benito (3.4 m yr^{-1}), Fraenkel (2.4 m yr^{-1}) and Acodado glacier. These glaciers are all located on the western side of the ice field. The most significant glacier retreat on the eastern side of the NPI was observed in Colonia glacier, with a distance of 1 km. The ice field lost a total of 50.6 km^2, representing a loss of 1.3%. They suggested that the shrinkage in the NPI glacier is first controlled by atmospheric warming after which local conditions come into play.

Willis et al. (2012) studied the ice loss rates in the NPI from 2000 to 2011 using satellite images from ASTER and SRTM. ASTER DEM was compared to SRTM DEM to obtain surface elevation difference of the ice field. ASTER DEMs that were generated by using the band 3N and band 3B of the ASTER images were acquired from the Land Processes Distributed Active Archive Center. Velocity maps for the glaciers were produced using sub pixel correlation from ASTER optical image pairs. They noted that thinning rates of glaciers have accelerated in lower elevations. They observed rapid thinning rates at the western side of the ice field compared to the eastern side. HPN 1 glacier experience the maximum thinning rates of -4.69 ± 0.95 myr^{-1}and Acodado glacier recorded thinning rates of -3.56 ± 1.16 myr^{-1}. Comparing the study of Willis et al., (2012) to Rivera et al., (2007), the thinning rates of HPI glacier and Acodado glacier increased from -4.00 ± 0.97 myr^{-1} to -4.69 ± 0.95 myr^{-1} and from -4.00 ± 0.97 myr^{-1} to -3.56 ± 1.16 myr^{-1} respectively after 10 years. They indicated that the front of San Quintin Glacier experienced the largest volume loss due to thinning. They summed the surface elevation changes of all the glaciers in the NPI to obtain a volumetric change of -4.06 ± 0.11 km^3 yr^{-1}, excluding volume loss caused by frontal retreat and sub-aqueous melting. They concluded that the total mass loss is 3.40 ± 0.07 Gtyr^{-1}, with at least 0.009 ± 0.0002 mmyr^{-1} of water being contributed to sea level rise.

Pellicciotti et al. (2013) provided a systematic review of the glacier changes in the Andes of Chile. They also used an advanced mass balance model that was previously used on the best monitored glacier (Juncal Norte Glacier) in the Andes to address modeling issues that need to be addressed in order to assess glacier changes. They used an energy balance (EB) model and an enhance temperature index (ETI) model in the

mass balance study. The EB model used air temperature, relative humidity, wind speed and direction, incoming and reflected shortwave radiation, incoming and outgoing longwave radiation, and aerodynamics surface roughness as inputs for the model. The ETI model only requires air temperature and net shortwave radiation flux as inputs. The two models are simulated for ablation seasons from 2008 to 2009. The ETI model is simulated a using non-parametric model, which considers the interaction between the solar beam and the topography and the transmission of the solar beam through the atmosphere. They obtained a mean cumulative ablation of 0.643 m.w.e. with the ETI model and a 1.469 m.w.e with the EB model for the Juncal Norte Glacier. They noted that the EB model simulates higher melt compared to the ETI model. They stated that wind speed and direction is difficult to model, even though they play a major role in snow re-distribution. As such, not taking into account these phenomena in mass balance models will introduce inaccuracies in mass balance results.

They also investigated the contribution of avalanching to mass balance figures in Juncal Norte Glacier by using the ETI model coupled with snow redistribution routine. They noticed that avalanches produce a varied pattern in mass balance. A more positive mass balance was observed at regions that received re-distribution from the avalanche. Mass balance figures change from positive to negative at regions that had ice re-distributed. To investigate the uncertainty in future mass balance predictions, they used the ETI model coupled to an accumulation and glacier runoff component. They noted that the uncertainty in climate models affects the uncertainty of the response of glaciers in terms of mass balance. However, uncertainties in the future climate are necessary for the projection of future glacier responses.

Schaefer et al. (2013) studied the climatic conditions and the surface mass balance in the North Patagonian Ice Field for the past and future using simulations from NCAR/NCEP Reanalysis and ECHAM5 global circulation data. A weather research model, a forecasting regional climate model and a sub-grid parameterization were used in rationalizing the ECHAM5 and NCAR/NCEP data to a resolution of 5 km. This 5 km downscaled data was further scaled down to a 450 m resolution, using temperature, precipitation and clear-sky radiation calculation on a finer grid as constants to a sub-grid parameterization. The surface mass balance model was calibrated using point and geodetic mass balance measurements on three large non-calving glaciers (HPN-1, HPN-4 and Exploradores) in the NPI, which was then applied to the other glaciers to obtain the net mass balance. The inputs to the model included incoming solar radiation, approximation of long-wave radiation and turbulent fluxes with a temperature function. The values from the models were validated with the Chilean Weather Service temperature and precipitation data, the Chilean Water Directory precipitation data, and the Chilean Navy and Argentine Weather Service data. They noticed an underestimation in their temperature values and corrected them with an amplitude of 2°C. An overestimation of precipitation was observed in most cases, which was corrected with a global precipitation correction factor of P_{corr}<1. They recorded an increase in accumulation in the NPI between 1990 and 2011 when compared to 1975 to 1990. They noted high thinning rated in the western side glaciers, especially in HPN-4 and HPN-1, with -2.16 m.w.e and -0.69 m.w.e respectively. Explorades glacier recorded -0.77 m.w.e. They indicated that the loss of ice through calving doubled in 2000 to 2009 than from 1975 to 2000, due to the precipitation as rain rather than snow at the tongues of the

glaciers. The model projected an increase in ablation from year 2050 whiles solid

precipitation will reduce from year 2080 due to high temperatures in the region. They

stated that during the 21st Century, 592±50 Gt of ice was lost. They indicated that there

are high uncertainties in the future prediction of mass balance due to uncertainties in

climate prediction, ice dynamics and snow drift.

Glacier retreat and lake expansion in the NPI

Most of the glaciers in the NPI are experiencing retreat since the Little Ice Age,

with the exception of some advances in glacier experienced in the 1990s (Rivera et al.,

2007). Aniya and Enomoto (1986) studied the behavior of the glacier outlets for the

periods of 1944-1974, and 1974-1985 using aerial photographs and ground survey. They

noticed a general retreat pattern of all the glaciers but also noted some glacier advances in

San Rafael and San Quintin glacier between 1935 and 1950. They also stated that there

are variations in the behavior and retreat rates in each of the glaciers, which they

attributed to topoclimatic and topographic effects. Aniya (1992) states that land-

terminating glaciers such as HPN-1 retreats at mean rates of at least 180 ma^{-1}, while

calving glaciers such as San Rafael experienced retreats as high as 300 ma^{-1} in the late

1980s.

Aniya (1999) studied the variations of 22 glacier outlets in the NPI between

1944/45 and 1995/96. The data he used for this study was a number of his own hand-held

oblique aerial photographs, trimetrogon oblique aerial photographs, vertical aerial

photographs, 1:50,000 Chile topographic maps, Landsat MSS and Landsat TM images

and SPOT images. By using the Landsat TM images as reference he digitized the aerial

photographs to compute the change in area. He found the frontal area retreat of the

glaciers to be a total of 64 km^2 and the total ice loss for the 51 year period to be 152 - 310 km^3. He noted that San Quintin and San Rafael glaciers experienced the maximum retreat, followed distantly by Cachet, Steffen and Nef glaciers. He stated that recently, San Quintin glacier lost mass through retreat at the glacier tongue and down-wasting. He noticed high retreat rates for the period of 1986 to 1991, but retreat rates were reduced and there were advances in some glaciers after 1991. It was reported by Winchester and Harrison (1996) that San Quintin glacier advanced by 150 m between 1991 and 1993. San Rafael glacier also experienced drastic retreats between 1975 and 1991, but retreat halted after 1991 and advances were recorded in 1992 by Warren and Sudgen (1993). Nef glacier on the contrary showed no stagnancies or advances between 1991 and 1994. It rather continued with rapid retreats until 1996, since the glacier tongue disintegrated into a proglacial lake in 1994. He assumed that the increase in precipitation during the 1979s influenced the reduction in retreat and advancement in some glaciers. Aniya and Sato (1996) gave the time lag for the response time for glaciers as 20 years in the NPI. Therefore the assumption by Aniya (1999) could be true. He stated that the thinning rates of glaciers on the west side (0.052 km^2 yr^{-1}) of the NPI are more than those of the east side (0.026 km^2 yr^{-1}) of the NPI. He indicated that the climatic data from the Chilean and Argentinean meteorological stations close to the ice fields recorded a slight increase in air temperature with a decrease in precipitation for the 40 to 50 years before the study. This would have caused the reduction in area of the glaciers.

Lopez et al. (2010) estimated the fluctuations of 15 glaciers in the NPI between 1945 and 2005, with 1945 aerial photographs compared to ASTER and Landsat satellite images. They observed a general retreat trend in all the glaciers, with San Rafael (5.7

km), Cachet (5.1 km) and Nef (3.4 km) glaciers experiencing the maximum retreat. They observed that San Quintin and San Rafael glacier showed no change until 1979 when they started a rapid retreat. The other glaciers that were retreating before 1979 also accelerated in retreat after 1979. They indicated that San Rafael glacier retreated approximately 3.3 km between 1979 and 1987. No clear relationship was found between glacier retreat and glacier size. They suggested that the retreat of the glaciers is controlled first by atmospheric warming from a global point of view followed by local conditions.

Loriaux and Casassa (2013) studied the evolution of glacial lakes in the NPI between 1945 and 2011 by digitizing glacial lakes from Llibourty's topographic map and multitemporal Landsat satellite images. They recorded an increase in glacier lake area of 66.0 km^2 for the study period. Their total lake area for 2011 was 167.5±8.4 km^2, compared to 101.6±19.1 km^2 in 1945 representing a total increase of 64.9%. San Quintin Lake experienced the most expansion with 18.0 km^2. They estimated the lake-area increase rate as 1.0 km^2 yr^{-1} for the 66 year period. They noticed some glacier stability between 1945 and 1987, which is in agreement with Aniya and Enomoto (1986), who also reported advances in San Rafael and San Quintin glacier between 1935 and 1950. They stated that the expansion of glacier lakes really increased after 1987.

Despite the gradual increase in the number of studies during the last few decades, there are still glacier mass balance inventories missing in the North Patagonian Ice fields. Due to the less attention given to the NPI, glacial lakes located in this region are barely monitored, which can lead to a disastrous outburst without prior warning.

Glacial lake outburst floods

Glacier Lake Outburst Floods (GLOF) is a disastrous discharge of large volume of water, by the breaking of moraine dammed lakes (Yamanda and Sharma, 1993). Glacier lakes form due to melting of glacier ice and snow. High rates of melting have increased the threat of glacial lake outburst in high mountain range of the world (Huggel et. al., 2002). Various natural phenomena such as avalanche, earth quake or even the weight of water itself breaks the moraine dams. There are several GLOF events in Andean glacial lakes. An example is the late 2000 GLOF in the North Patagonia Ice field, where a rock fall partially displaced Lake Lago Calafate and caused an outburst (Harrison et. al., 2006).

These outbursts repeatedly cause loss of human lives as well as severely damaging cropland and property in different parts of the world (Clague and Evans, 2000, Richardson and Reynolds, 2000). In the tropics, moraine-dammed lakes are most popular in the Peruvian Andes and the Cordillera Blanca (Huascaran Massif) (8º - 10ºS) (Ames, 1998), and there has been reports of devastated outbursts in these areas (Reynolds, 1992) especially in the course of the twentieth century (Carey, 2005).

Air and space-borne remote sensing provides a means of assessing the hazard caused by GLOF (Kaab et al., 2005). Spatial resolution of space-borne sensor images for glacier and permafrost hazards limits their accuracy and application in hazards study (Kaab et al., 2005). The availability of data from high-resolution sensors such as IKONOS, QuickBird or Orbview3 makes accurate GLOF hazard monitoring a possibility, but are very expensive and only able to cover small areas (Fischer et al., 2006). However, glacial lakes studies with Landsat images have proven successful.

28

Loriaux and Casassa (2013) measured the evolution of glacial lakes in the NPI using Landsat images and topographic maps between 1945 and 2011. They indicated an increase in the total glacial lake area from 101.6 ± 19.1 km^2 in 1945 to 165.5 ± 8.4 km^2 in 2011 representing an increase of 64.9%, with San Quintin Lake experiencing the maximum expansion within the time period.

This chapter discussed the different methods of mass balance measurements, DEM creation and accuracy, satellite images for mass balance and glacial lakes expansion studies previous glacier studies in the NPI and GLOFs. Chapter 3 discusses the data, techniques and methods applied in this study

CHAPTER III

RESEARCH METHODOLOGY

This chapter will discuss the remotes sensing method of mass balance estimation of the 13 glaciers that were studied within the NPI. The data, detailed analysis and statistical tests in the execution of the two research objectives will be presented.

Mass balance estimation of 13 glaciers in the NPI using remote sensing techniques

The remote sensing technique adopted in this research uses the difference in elevation values, extracted at pixel level from DEMs for at least two different time periods. The mean elevation value for each individual glacier is then multiplied by the density of ice, commonly known as 900 kg. m^{-3} (Paterson, 1994) and divided by the number of years within the time period of the study. This value shows the mass balance of the glacier per annum. To obtain the meter water equivalent (m.w.e.a^{-1}), the mass balance value is divided by the density of water (1,000 kg.m^{-3}).

Usually, satellite images that have stereoscopic capabilities are used for mass balance studies. This is because DEMs can be generated from them, so that elevation changes can be computed (Berthier et al., 2007). In generating the DEM, GCPs are mostly required. But due to the unavailability of GCPs in most cases, topographic maps acts as base maps for GCPs extraction (Wang et al., 2005).

Dataset

ASTER

Two ASTER images with the dates April 4th, 2007 and March 18th, 2012 were

used in this study. ASTER satellite images were used because it has the stereoscopic

capability to generate DEMs. ASTER is a high multispectral imager, which was launched

in December 18, 1999 on the National Aeronautics and Space Administration's (NASA)

terra satellite by NASA and Japan's Ministry of Economy (Yamaguchi et al., 1998).

ASTER consists of 14 bands in 3 systems which handles different spectral regions. These

are the visible and near infrared (VNIR), shortwave infrared (SWIR), and thermal

infrared (TIR), with spatial resolution of 15, 30 and 90 respectively (Muukkonen and

Heiskanen, 2007) (Figure 3.1). One ASTER image covers an area of 60 X 60 km^2

(Hirano et al., 2003). Two ASTER bands make it possible for DEM creation. These are

the band 3N and band 3B, which are the Nadir and the backward-looking telescopes on

the NIR wavelength (Hirano et al., 2003). They have wavelength range of 0.78 to 0.86

μm. Besides the standard level 1A and level 1B data produced by ASTER, level 2 data

products which are of higher-order and contain atmospherically corrected surface

reflectance and radiance data (Abrams, 2000) are also produced by ASTER. Each of the

ASTER images were projected to WGS84 datum, UTM Zone 18S because this is the

UTM coordinate system that the NPI falls into.

Subsystem	Band No.	Spectral Range (μm)	Spatial Resolution, m	Quantization Levels
VNIR	1	0.52-0.60	15	8 bits
	2	0.63-0.69		
	3N	0.78-0.86		
	3B	0.78-0.86		
SWIR	4	1.60-1.70	30	8 bits
	5	2.145-2.185		
	6	2.185-2.225		
	7	2.235-2.285		
	8	2.295-2.365		
	9	2.360-2.430		
TIR	10	8.125-8.475	90	12 bits
	11	8.475-8.825		
	12	8.925-9.275		
	13	10.25-10.95		
	14	10.95-11.65		

Figure 3.1   Characteristics of ASTER Sensor Systems

Source: ASTER User Handbook Version 2

Topographic map

Twelve topographic maps of 1:50,000 scale created by the Istituto Geografico Militar of Chile (IGM) in 1979 were purchased from East View Geospatial Company. The contour intervals in these maps is 50 m. Falkner, (1995) estimated the vertical random error of this map to be 17 m. The National Imagery and Mapping Agency (NIMA, 1997) estimated the horizontal error as 15 m. These topographic maps were projected to WGS 1984 UTM Zone 18S.

Global Land Ice Measurements from Space (GLIMS)

The GLIMS project is internationally collaborated, which collects satellite images of the world for glacier studies. Its goal is to create a global inventory of glaciers, analyze glacier changes and investigate the causes and effects of these changes (Kargel et al., 2005). Data from the GLIMS database can be downloaded at "http://nsidc.org/glims/".

Within the GLIMS database, users can browse for different custom maps, display and query and download information (Raup et al., 2007). The world glacier boundaries can be downloaded from the database.

DEM creation

The OrthoEngine extension of PCI Geomatica 2012 software was used in the DEM creation. The band 3N and band 3B of the ASTER Level 1A were used to generate multi-temporal DEMs. To do this, 50 well distributed GCPs and 100 well distributed Tie Points (TPs) were collected in the 2007 image and the 2012 image. In collecting the GCPs and the TPs, the same pixel is identified in the band 3N and 3B in each image. A point is then fixed for this location (Figure 3.2). This was repeated for 50 different locations for the GCPs collection and 100 different locations for the TPs.
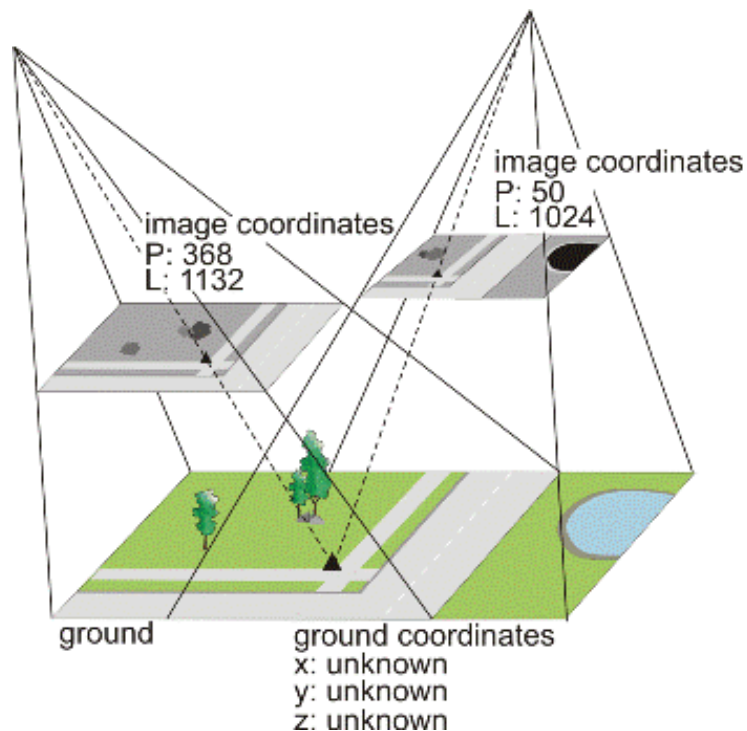
Figure 3.2   The representation of TPs in stereo pair images

Source: PCI Geomatica manual 2012

During the GCPs and TPs collection, priority was given to exposed rocks, mountain peaks and non-glaciated region since they hardly change unless there is a natural disaster. Glaciated areas, shaded areas and cloud-covered areas were excluded in GCPs, as they are highly variable and could introduce inaccuracies in the DEM. The RMSE after the GCPs collection was 2.14 m for the 2012 image with and X RMSE of 1.81 m and a Y RMSE of 1.13 m. The RMSE for the 2007 image was 1.37 m with and X RMSE of 1.03 m and a Y RMSE of 0.90 m. The DEMs were generated using PCI Geomatica 2012. Elevations for the GCPs were extracted from a 1:50,000 topographic map and the AGDEM.

The TPs assisted in orienting the stereoscopic images (3N and 3B) and defined epipolar geometry for the images during the extraction of the DEM. So after the TPs are collected epipolar images are created (Figure 3.3), where PCI geomatica orients the images such that the TP locations on the band 3N and band 3B have the same coordinates (PCI Geomatica manual, 2012). The DEM was generated after the epipolar images were created. A DEM each was generated for the 2007 and the 2012 image. These DEMs were projected to UTM Zone 18S.
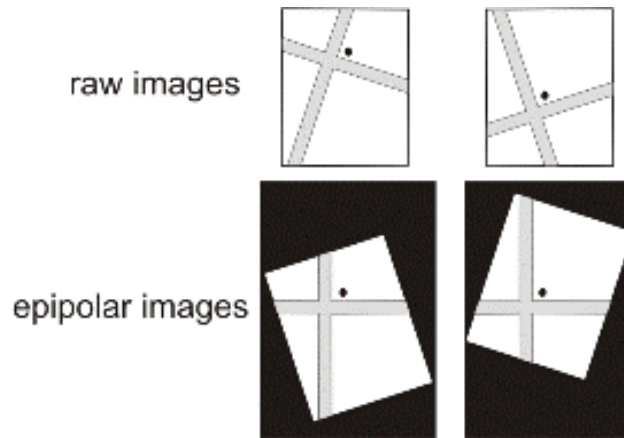
Figure 3.3   Epipolar generation

Source: PCI Geomatica manual 2013

Digitizing glacier boundary

In order to separate the glaciated area from the non-glaciated area, the glacier boundary is digitized on the ASTER 2012 image, with the Global Land Ice Measurements from Space (GLIMS) boundary as reference using the ArcGIS 10.1 software. The boundary is digitized on the ASTER 2012 image because it is the most recent image in this analysis, so it was made the base image. The overlapping regions between the 2012 and the 2007 images were digitized and used for the mass balance analysis (Figure 3.4). This is because elevation difference between images can only be calculated if there are at least two common regions between the images. Fourteen glaciers fell within the overlapping region namely; San Quintin, Fraenkel, Strindberg, Colonia, Acodado, HPN 1, HPN-4, Cachet, Cachet Norte, Nef, Arco, Benito, Pared_Norte and U5. Pared Norte glacier was excluded from this analysis because only a very small area of the glacier fell within the overlapping region.
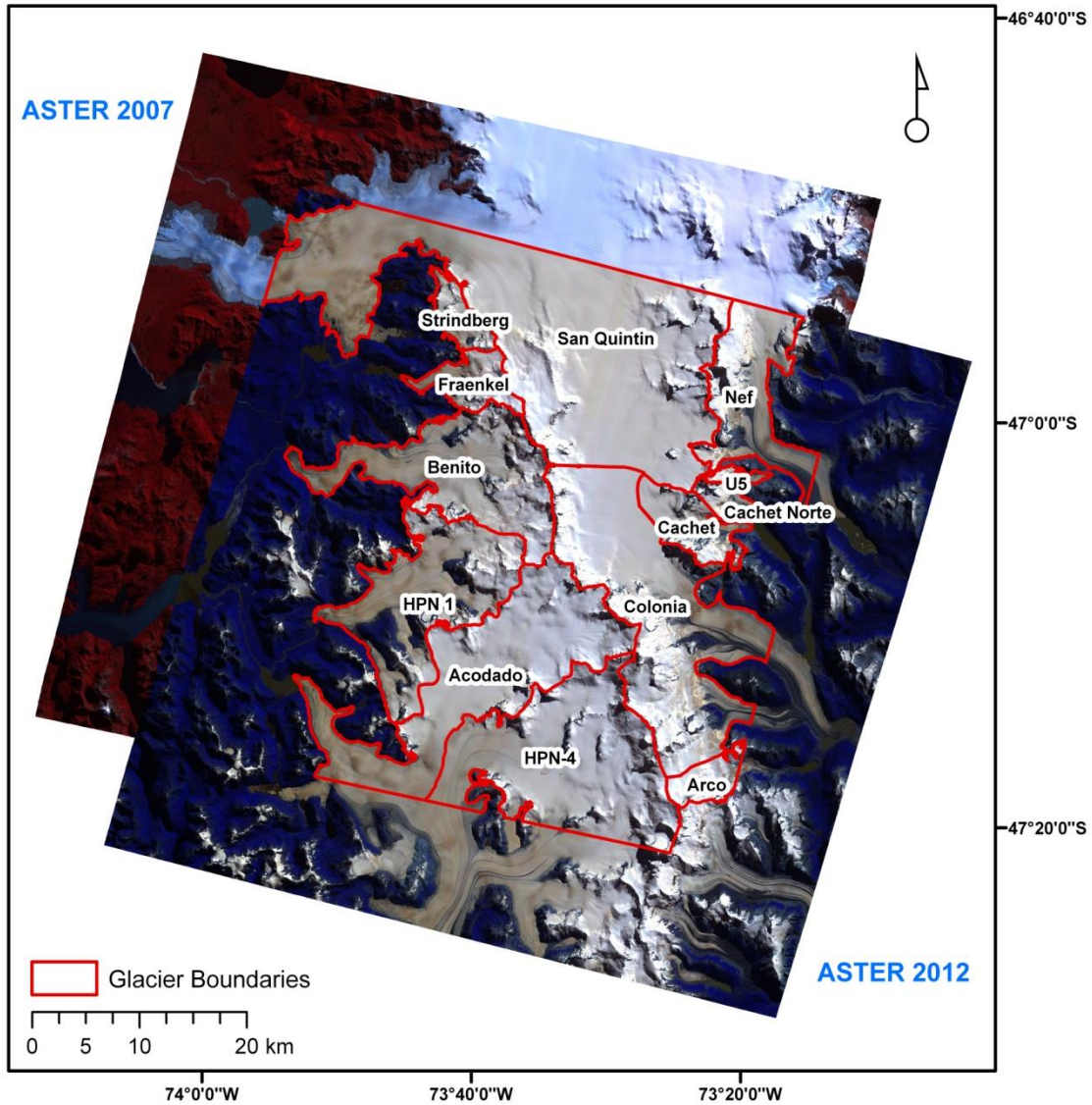
Figure 3.4   Glaciers within the overlapping region of the ASTER 2007 and ASTER 2012, analyzed in this study

Elevation difference by using random points

The change in elevation values can be computed by finding the difference in DEM values between the 2012 image and the 2007 image. By doing this, the entire DEM area common to both images are taken into account. This will introduce inaccuracies in

the final mass balance value. This is because even though high slope, shaded and cloud cover areas were excluded during the TPs collection, there are still areas that have pixel values completely off compared their surrounding pixels.

In order to eliminate these areas, the random points generation technique is adopted. This is where random points are created all over the common DEM area. One million random points are generated at 21.22 meters; the hypotenuse is the square root of 15m X 15m square pixels. This distance was chosen to make sure that no two random points lie within the same pixel since the pixel size is 15 m. Elevation values were extracted to the random points from both images using "Extract Multi Values to Points" in ArcGIS 10.1 in both glaciated and non-glaciated areas. Elevation values on the random points of the 2012 image are subtracted from the values of the 2007 image. Random points with elevation difference values greater than 150m and less than -150 are eliminated.

It is expected that the non-glaciated region should have a zero elevation difference value, since there should be no change in elevation unless there is a natural disaster. Most of the elevation difference in the non-glaciated region had non-zero values associated with them. This means that there are also vertical errors in the glaciated region. Therefore this vertical error needs to be corrected in order to get accurate mass balance results in the glaciated region. To reduce vertical errors, DEM values of 2012 images were de-trended by reducing the Standard Deviation (STDV) and Mean Elevation Difference (MED) values in glaciated areas. This was done by subtracting the STDV value (25.91 m) in the non-glaciated from the positive elevation values in the glaciated region of the 2012 DEM, and adding 25.91 m to the negative elevation values.

37

Uncertainty estimation

Relative uncertainties in the elevation difference in glacier and non-glacier areas were computed using their individual Standard Error (SE) (Bolch et al., 2011). SE in the non-glaciated area is calculated with the equation below, where 'n' is the number of included pixels.

$$SE = \frac{\text{STDV non} - \text{glac}}{\sqrt{n}}$$
3.1

The SE and the MED of the non-glaciated area were used to calculate the uncertainty in glaciated areas accordance with the law of error propagation (Bolch et al., 2011).

$$e = \sqrt{(SE)^2 + (MED)^2}$$
3.2

e = uncertainty

In order to obtain the mass balance for each of the glaciers, the mean elevation difference was multiplied by the density of ice (900 kg.m^{-3}). Mass balance was finally presented as m w.e.a^{-1} (Bolch et al., 2011, Ambinakudige and Joshi, 2013).

DEM accuracy test and t-tests

The elevation of the master DEM (2007) was compared with the elevation of the 1:50,000 scale topographic maps. To do this, 70 well distributed random points were created on the non-glaciated region of the master DEM. Elevation values were then extracted from the master DEM with the random points. These elevation values are then compared with the elevation values of the topographic map by computing the SE and Uncertainty (*e*) in dataset using equation (3.1) and (3.2).

An paired statistical t-tests were performed to determine the significance of the data. The first pair of statistical t-test was performed by comparing the mean elevation of the glaciated region of the master DEM (2007) with the mean elevation of the glaciated region of the 2012 DEM. The second pair of statistical test evaluated the mean elevation of the non-glaciated region of the master DEM and the mean elevation of the non-glaciated region of the 2012 DEM.

Volume change and mass balance calculation

In order to obtain the mass balance, the mean elevation difference of each glacier is multiplied by the density of ice (900 kg m^{-3}) and divided by 5 (number of years between 2007 and 2012), resulting in the mass balance kg m^{-2} yr^{-1}. Depending on geographical location, climatic influences, altitude, amount of accumulation and ablation area, the mass balance of glaciers that are close to each other or even share boundaries may vary in mass balance values. The mass balance values are converted to meter water equivalent per annum by dividing the mass balance by the density of water (1,000 kg m^{-3}).

Measurement of glacier retreat and expansion of glacial lakes

Dataset

Three Landsat images and 1979 1:50,000 topographic maps were used to measure the retreat of the NPI glaciers, and to analyze the expansion of glacial lakes. The Landsat images were the 1985 (Landsat 5 TM), 2000 (Landsat 7 ETM+), and 2013 (Landsat 8) images. The Landsat images were downloaded from USGS EROS website

(http://earthexplorer.usgs.gov). Both image types were re-projected to WGS 84 UTM Zone 18S.

Landsat

There are three types of Landsat images; Landsat MSS (Multispectral Scanner), Landsat TM (Thematic Mapper) and the Lansat ETM+ (Enhanced Thematic Mapper Plus). The spatial resolution of the Landsat MSS image is 57 x 79 m. It has five spectral bands (2 visible bands, 2 near infrared bands and 1 thermal band). The Landsat ETM+ image has spatial resolution of 28.5 m and has 7 spectral bands (3 visible bands, 1 near infrared band, 2 short infrared bands and 1 thermal band).

The Lansat image types used in this study were the Landsat TM and the Landsat ETM+. The earliest available Landsat TM image that was cloud-free was acquired on March 7th, 1985. The next was a Landsat ETM+ image for March 8th, 2000 and then Landsat 8 image for September 28th, 2013. The 30 meter resolution Landsat images have been orthorectified by the Global Land Cover Facility of University of Maryland (GLCF) and the United States Geological Survey (USGS). The absolute error estimated for these images are less than 50 m (Rivera et al., 2007). All the images were georeferenced with the parameters in Table 3.1.

Table 3.1   Projection information used to georeference aforementioned satellite images
            and topographic maps

Projection	Universal Transverse Mercator
Projected Coordinate System	WGS_1984_UTM_Zone_18S
False coordinate of origin	500000m Easting; 10000000m Northing
Central Meridian	-75
Scale factor at Central	0.9996

Glacier retreat measurement in the NPI

Retreats of nine glaciers in the NPI were measured between 1979 and 2013 in this study (Figure 3.5). These glaciers are San Rafael, San Quintin, Colonia, Acodado, HPN-1, Nef, Strindberg, Fraenkel and Pared Norte. The retreat was recorded by measuring the change in the position of the tongue of the glacier during the study period (Lopez et al., 2010).
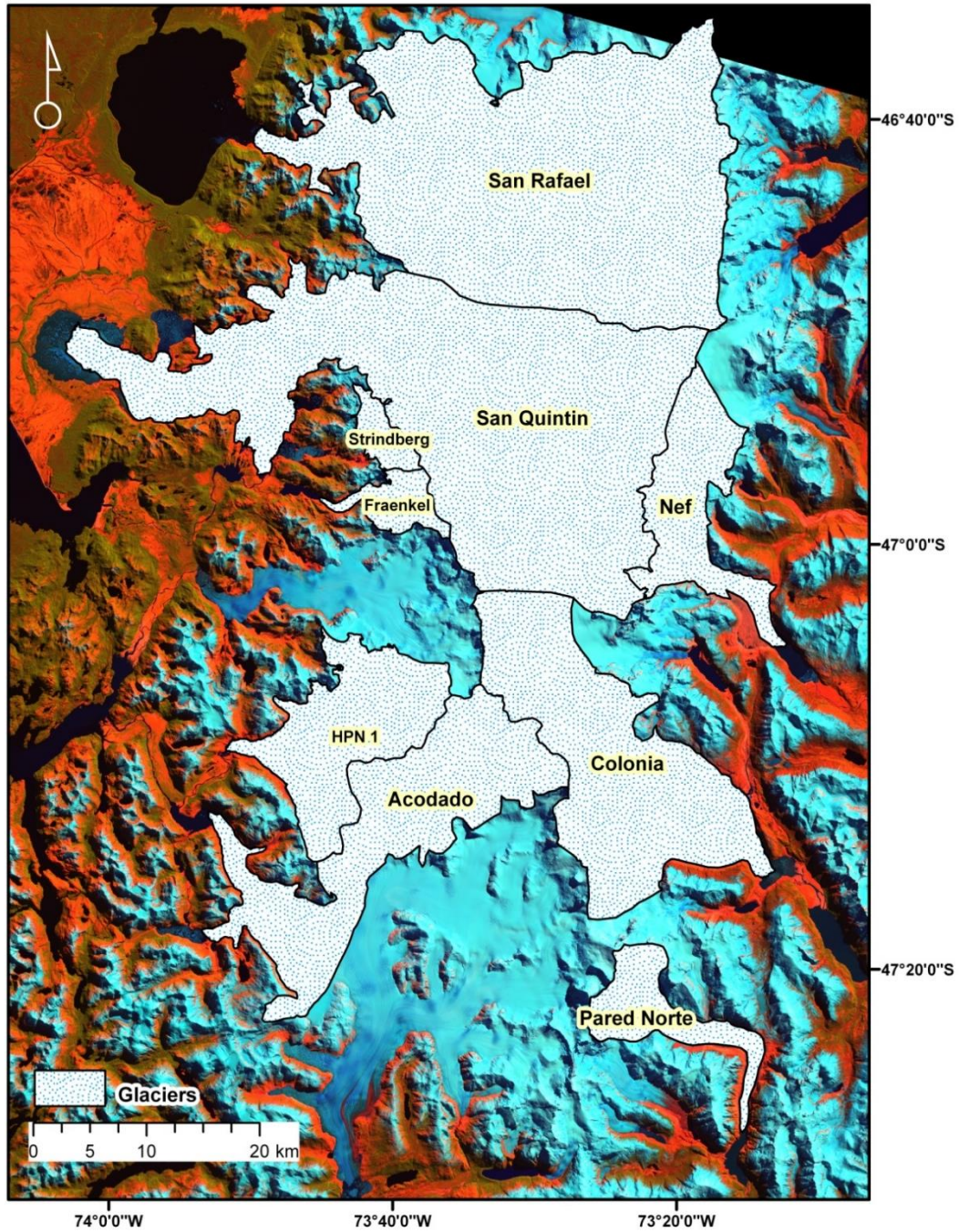
Figure 3.5   Glaciers considered in the retreat study.

Source: Glaciers digitized from Landsat 8 image (Band 6, Band5 and Band 2).

Expansion of glacial lakes measurements

Six glaciers consisting of 9 glacial lakes initially in 1979 were considered in the glacial lake expansion study (Figure 3.6). These lakes are found at the tongue of San Quintin, Fraenkel, Nef, Acodado, Cachet and Benito glaciers.
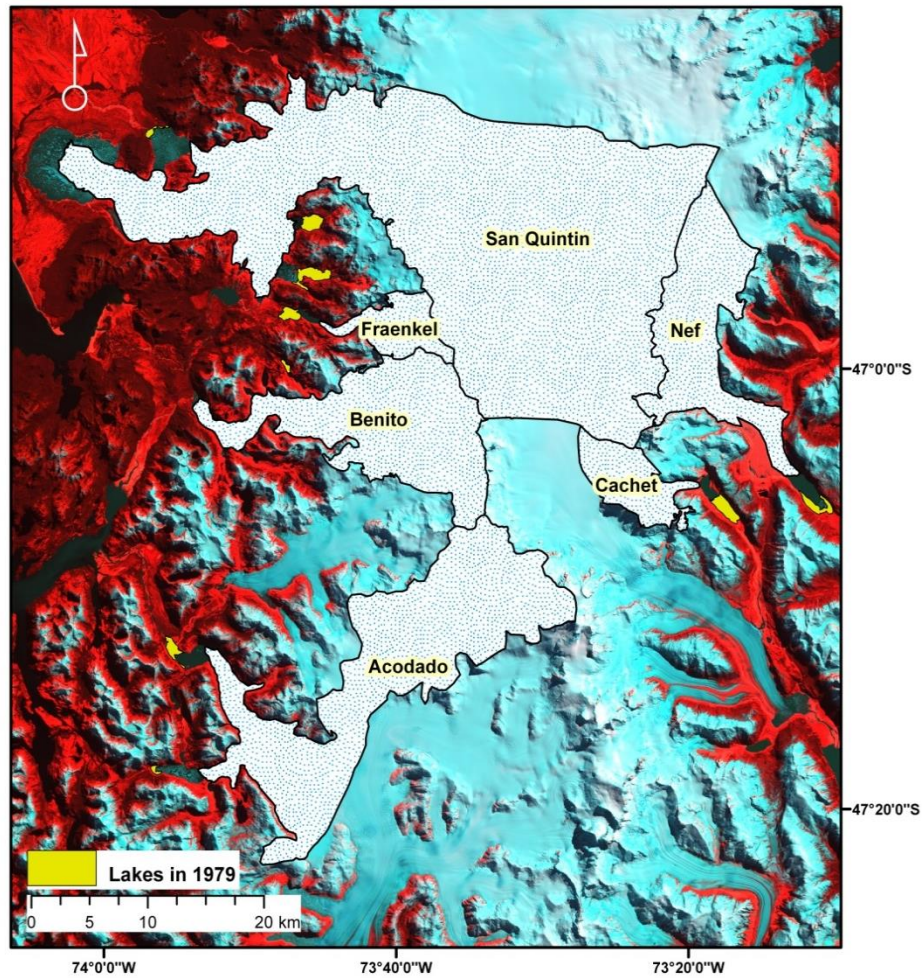
Figure 3.6   Glacial lakes considered in lake expansion study.

Source: Glaciers and lakes digitized from Landsat 8 image (Band 6, Band 4 and Band 1)

To clearly delineate the glacier lakes, the Normalized Differenced Water Index (NDWI) was employed along with visual/manual interpretation by using various band combinations (Ambinakudige, 2010). The NDWI uses the (Near Infrared) NIR and Blue band to differentiate water bodies from other features (Huggel et al., 2002).

$$NDWI = \frac{B_{NIR} - B_{blue}}{B_{NIR} + B_{blue}}$$ 3.3

With the NDWI and the Landsat images, the glacier lakes within the NPI are digitized with the ArcGIS 10.1 software. The topographic map is also digitized. A change in lake area is clearly observed from 1979 to 2013, which is a 34 year period.

CHAPTER IV

RESULTS AND DISCUSSION

Sections 4.1 to 4.2 of this chapter will explain the research results of the study in fulfillment of the study objectives of this study, stated in Chapter I. The specific study objective were:

1. To estimate mass balance of major glaciers in North Patagonia Ice Field between 2007 and 2012 using remote sensing techniques.

2. To measure the multi-decadal retreat of the North Patagonian glaciers and

3. to analyze the expansion of glacial lakes using topographic maps and Landsat (TM, ETM+ and 8) images between 1979 and 2013.

Estimation of mass balance of major glaciers

The accuracy of the master DEM was validated with the topographic maps by computing the MED, STDV, SEM and uncertainty presented in Table 4.1.

Table 4.1   Uncertainty calculation of master DEM with respect to topographic Map

Error Analysis of 2007 DEM with respect to Topographic Map	
Number of elevation points (n)	70
Mean Elev. Difference (m)	-24.2
Avg. STDV	60.65
Standard Error (SE)	7.8
Uncertainty (e)	24.2
Minimum elevation	-141
Maximum elevation	136

The MED, STDV, SE and uncertainty were calculated using elevation values from the non-glaciated region. The results are presented in Table 4.2.

Table 4.2   Descriptive statistics of non-glaciated area

Mean	-10.89
Std. Error of Mean	0.08
Std. Deviation	25.91
Number of random points	105109
Uncertainty (e)	10.89
Minimum elevation	-149
Maximum elevation	149

Based on the non-glaciated region parameters, uncertainty in mass balance of glaciated area was estimated to be ± 1.96 m.w.e.a^{-1}.

The significance of the paired t-test was to show if there was a significance difference in elevation values between the glaciated regions of the 2007 DEM and the 2012 DEM and if there was a significant difference in the elevation values between the

non-glaciated regions of the 2007 DEM and 2012 DEM. The first pair of t-test results between the non-glaciated region should show no significant difference in elevation values since there should be no change in elevation unless there is a natural disaster. On the contrary, elevation differences were observed. Therefore, this vertical error was removed by de-trending. The paired t-test for the glaciated region showed statistical difference as expected. These t-test results are shown in Appendix A.

Mass balance values calculated for the period of 2007 to 2012 is present in Table 4.3.

Table 4.3   Mass balance of glaciers from 2007 to 2012 year period.

Name	Size (sq. km)	Mean Elev. Diff	Specific Mass Balance (m.w.e.a-1)
Arcodado	212.66	-12.8±10.89	-2.3±1.96
Arco	10.63	-40.05±10.89	-7.2±1.96
Benito	162.49	0.04±10.89	0.007±1.96
Cachet	42.32	10.51±10.89	1.89±1.96
Cachet Norte	11.57	10.87±10.89	1.95±1.96
Colonia	242.88	-6.85±10.89	-1.2±1.96
Fraenkel	32.73	9.72±10.89	1.74±1.96
HPN-4	203.39	-49.52±10.89	-8.9±1.96
HPN 1	167.61	-9.34±10.89	-1.6±1.96
Nef	77.15	55.07±10.89	9.91±1.96
San Quintin	423.52	26.49±10.89	4.76.±1.96
Strindberg	21.16	19.87±10.89	3.57±1.96
U5	5.42	15.66±10.89	2.81±1.96

HPN-4, Arco, Acodado, HPN-1 and Colonia, in descending order, experienced a negative mass balance. Nef, San Quintin, Strindberg, U5, Cachet Norte, Cachet, Fraenkel and Benito, in descending order, recorded a mass gain because most of their area was in the accumulation zone of the ice field. The study recorded a high uncertainty of ±10.89 m

in the mean elevation difference. This is due to the rugged nature of the ice field, unavailability of GCPs from the ice field and the high error in the topographic map. As such the DEMs that were generated were not of high quality. The ice field was divided into the East part, Middle part and West part, with the East and West parts being the ablation zone and the Middle part being the accumulation zone (Figure 4.1). This division is done based on an ELA of 1100 meters.
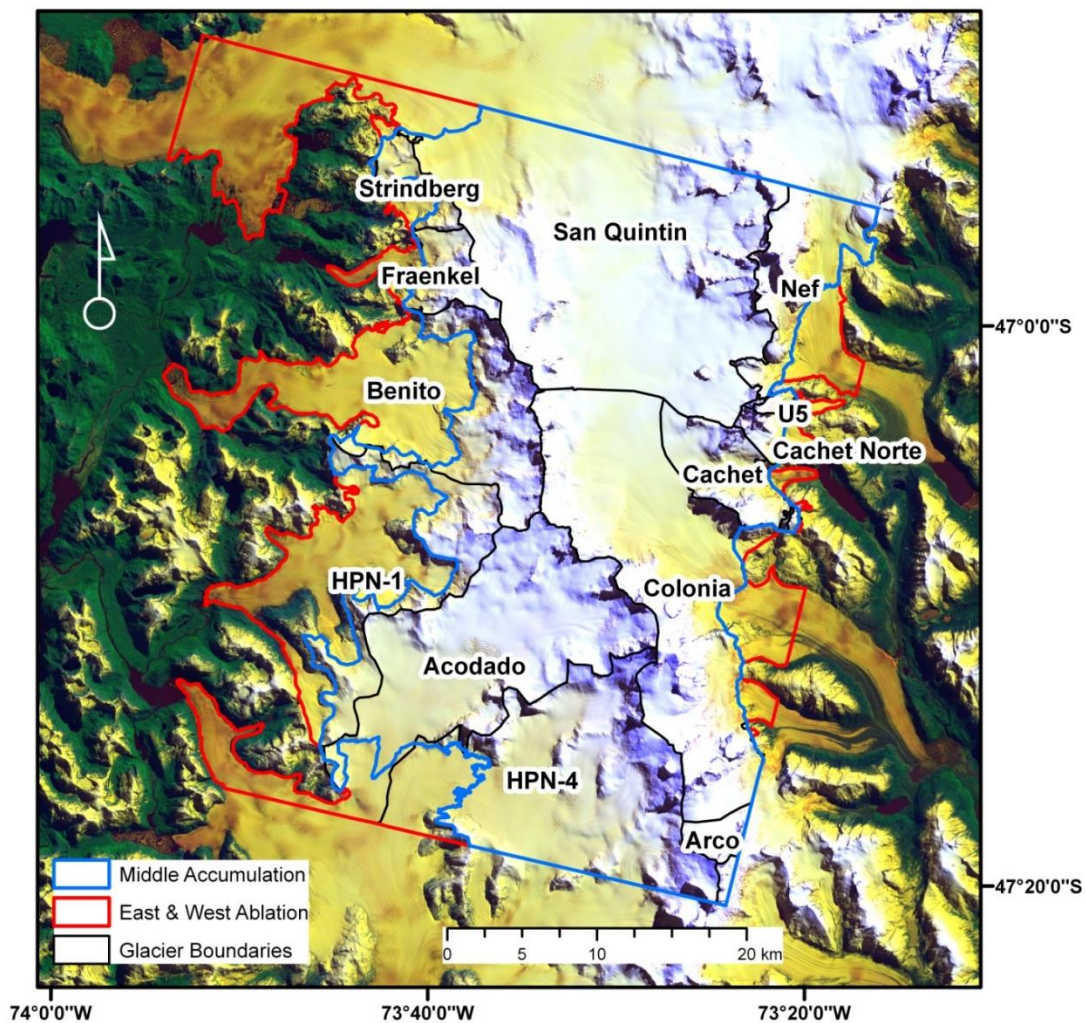
Figure 4.1   Glacier accumulation and ablation zones

Source: Digitized from Landsat 8 satellite image (Band 5, Band 3 and Band 1).

Mass balance values were calculated again for each of the glaciers, now dividing each glacier with respect to either East (Ablation), Middle (Accumulation) or West (Ablation) location as seen in figure 4.1. The result is presented in Table 4.4.

Table 4.4   Mass balance of glacier accumulation and ablation zones.

Glacier Location	Mean Elev. Diff	Specific Mass Balance (m.w.e.a^{-1})
Cachet Ablation	18.10±10.89	3.25±1.96
Cachet Accumulation	9.77±10.89	1.75±1.96
Cachet Norte Ablation	23.81±10.89	4.28±1.96
Cachet Norte Accumulation	1.87±10.89	0.33±1.96
Fraenkel Accumulation	17.82±10.89	3.20±1.96
Fraenkel Ablation	-5.56±10.89	-1.0±1.96
Colonia Ablation	-0.01±10.89	-0.0±1.96
Colonia Accumulation	-8.2±10.89	-1.4±1.96
Nef Ablation	58.02±10.89	10.4±1.96
Nef Accumulation	52.96±10.89	9.53±1.96
U5 Ablation	42.54±10.89	7.65±1.96
U5 Accumulation	-2.07±10.89	-0.3±1.96
HPN-4 Accumulation	-49.48±10.89	-8.9±1.96
HPN-4 Ablation	-49.71±10.89	-8.9±1.96
Benito Accumulation	5.87±10.89	-1.7±1.96
Benito Ablation	5.88±10.89	1.05±1.96
Acodado Accumulation	-8.96±10.89	-1.6±1.96
Acodado Ablation	-40.11±10.89	-7.2±1.96
HPN 1 Accumulation	-0.55±10.89	-0.0±1.96
HPN 1 Ablation	-13.09±10.89	-2.3±1.96
Arco Accumulation	±10.89±10.89	-7.2±1.96
San Quintin Accumulation	35.02±10.89	6.30±1.96
San Quintin Ablation	-0.04±10.89	-0.0±1.96
Strindberg Accumulation	26.21±10.89	4.71±1.96
Strindberg Ablation	10.39±10.89	1.87±1.96

It is not expected that all mass balance values of the glaciers that have been sectioned be positive or negative based on as to whether they fall in the ablation or accumulation zone. The ablation zone of Colonia glacier showed no change in mass

balance but the portion of Colonia glacier that fell in the accumulation zone I sectioned was another ablation zone of Colonia glacier and therefore showed a negative mass balance of -1.4 m.w.e a^{-1}. This mass balance value of -1.4 m.w.e a^{-1} is of high uncertainty of ±1.96 m. Therefore, even though a negative mass balance was recorded for Colonia's other ablation zone, the uncertainty value of ±1.96 m if applied, could make the ablation zone record stability or a negative mass balance. The accumulation zone of San Quintin glacier showed a positive mass balance of 6.30 m.w.e a^{-1}. But it cannot be said with high certainty that the ablation zone of San Quintin showed no change in mass balance even though it recorded -0.0 m.w.e a^{-1}. Heavy snow cover in the study region introduced error in mass balance estimation especially in accumulation areas. Mass balance records are more accurate in clear ice areas of the glaciers.

By categorizing the glaciers into these three sections, mass balance values can be determined accurately based on whether that part of the glacier is in an accumulation or ablation zone. Mass balance values determined for the overall area of the glacier is averaged over the accumulation and ablation zones. This causes an averaging of extreme ablation and accumulation zones that fall within one glacier. An example is the Fraenkel glacier, which has an overall positive mass balance of 1.74 m.w.e a^{-1} but when divided into accumulation and ablation zone recorded 3.2 m.w.e a^{-1} mass change in accumulation zone, and -1.0 m.w.e a^{-1} mass balance in ablation zone. With a ±1.96 m uncertainty in the mass balance values, a mass balance value of -1.0 m.w.e a^{-1} could either be more negative or record a gain of 0.96 m.w.e a^{-1}. This makes the division into accumulation and ablation zones very helpful in glacier mass balance analysis.

It can be said that not all glaciers are experiencing a linear trend in mass loss between 2007 and 2012. An example is the advancement of San Quintin glacier between 1991 and 1994 (Winchester and Harrison, 1996). Between 1996 and 1999, most glaciers in the accumulation region of the NPI showed advances (Harrison and Winchester, 1998). In spite of these advances, Rivera et al., (2007) obtained negative thinning rates in all the glaciers in the NPI between 1975 and 2001. These average ice loss rate have more than doubled to an equivalent sea level rise in the North and South Patagonian Ice fields between 1995 to 2000 (Rignot et al., 2003). Aniya, (1999) estimated the thinning rate of HPN-1 glacier as -0.7 m.w.e a^{-1} between 1945 and 1975, Rivera et al., (2007) estimated the thinning to be -4.0 m.w.e a^{-1} between 1975 and 2001, whilst we recorded a negative mass loss of HPN-1 to be -1.6 m.w.e a^{-1}. Glacier thinning is linear to mass balance loss. Therefore a reduction in negative mass loss can be attributed to more accumulation which could influence stable glaciers to become more positive. Schaefer et al., (2013) experienced the highest mass loss in HPN 4 glacier with -2.16 m.w.e between 1990 and 2011, while in this study HPN 4 recorded the highest mass loss of -8.9±1.96 m.w.e.a.$^{-1}$.

Glaciers on the western side of the nunataks experienced more mass loss than glaciers on the eastern side of the nunataks. Aniya, (1988) referred to orographic factors as the cause of this pattern. He further explained that the eastern side of the NPI receives less snow fall since the NPI lies in the zone of the westerlies. On the contrary, the eastern side receives more snow through drift snow that is blown by wind. Due to this reason, even though the eastern side receives less snow, it accumulates more snow due to drift snow and experiences less retreat in the NPI.

Lopez et al. (2008) also gives reasons for this pattern. They explained that the extent of snow coverage decrease in September as a result of increase in temperatures during summer seasons. Precipitation starts to decrease in August on the western side and in the eastern side, precipitation decrease starts in September. During this occurrence, high wind velocity at the same time tends to shift the distribution of snow eastward. They also state that snow cover on the western side is only affected by the seasonality in temperature because precipitations showed no seasonality. The snow cover on the eastern side on the other hand showed seasonality in both temperature and precipitation. They noted that the under this circumstance, snow will melt faster on the western side but will be quickly covered again with snow due to high precipitation in this region. Lower winter temperatures on the eastern side will cause snow to remain longer than on the western side. Due to this pattern, it is expected that the glaciers on the eastern side experience less melt than glaciers on the western side. This explanation reflects the mass balance results obtained in this study as the glaciers on the western side experienced more mass loss as compared to the eastern side.

By using a 95% confidence interval in the paired t-tests to examine the significant difference in elevation values in the glaciated region, the p-value was also computed. The p-value for the entire glaciated region as presented in Appendix A was zero. The rejection level for the null hypothesis is 0.05. Therefore, the null hypothesis can be rejected if the p-value is less than 0.05. Due to estimates above, the first null hypothesis that states that there was no significant mass change in glaciers in the North Patagonia Ice Field from 2007 to 2012 rejected. This is because even though there is high uncertainty in

the mass balance values, all the glaciers experienced a change in mass during the study period.

Glacier retreat and expansion of glacial lakes

The extents of retreat of all nine glaciers are shown are in Figure 4.3 to Figure 4.5. Table 4.5 shows the values of the retreat. San Quintin retreated the most by 4.5 km. Lopez et al., (2010) and Aniya, (1999) both recorded maximum retreats in San Quintin glacier. This is because, a glacier tongue that was fully ice in 1979 retreated by 4.5 km to form a new lake by 2013 (Figure 4.2). But another glacier tongue in San Quintin retreated by 3.03 km. San Rafael especially experienced retreat of about 3.3 km between 1979 and 1987 (Lopez et al., 2010). On the contrary, San Quintin retreated only by approximately 0.5 km within the same time period. Nef glacier followed San Quintin and San Rafael by recording a 3.82 km retreat. Aniya, (1999) also had Nef glacier retreat value follow San Quintin and San Rafael. Aniya, (1992) stated that land-terminating glaciers such as HPN-1 retreats at mean rates of at least 180 ma^{-1}. But during the 34 year period of this study, HPN-1 glacier retreated by 2.43 km, resulting in a 71.47 ma^{-1} retreat. Therefore, the retreat rate that was estimated for HPN-1 glacier by Aniya, (1992) was reduced according to the estimates from this study.

In general, all glaciers have retreated in the study area, and that could be attributed to atmospheric warming in this region (Lopez et al., 2010). The rate at which these glaciers retreat is a direct response to climate, since these glaciers are temperate glaciers and respond rapidly to change in temperature (Lliboutry, 1998). However, due to the lack of weather data in the study region, long term temperature changes could not be analyzed in this study.

53
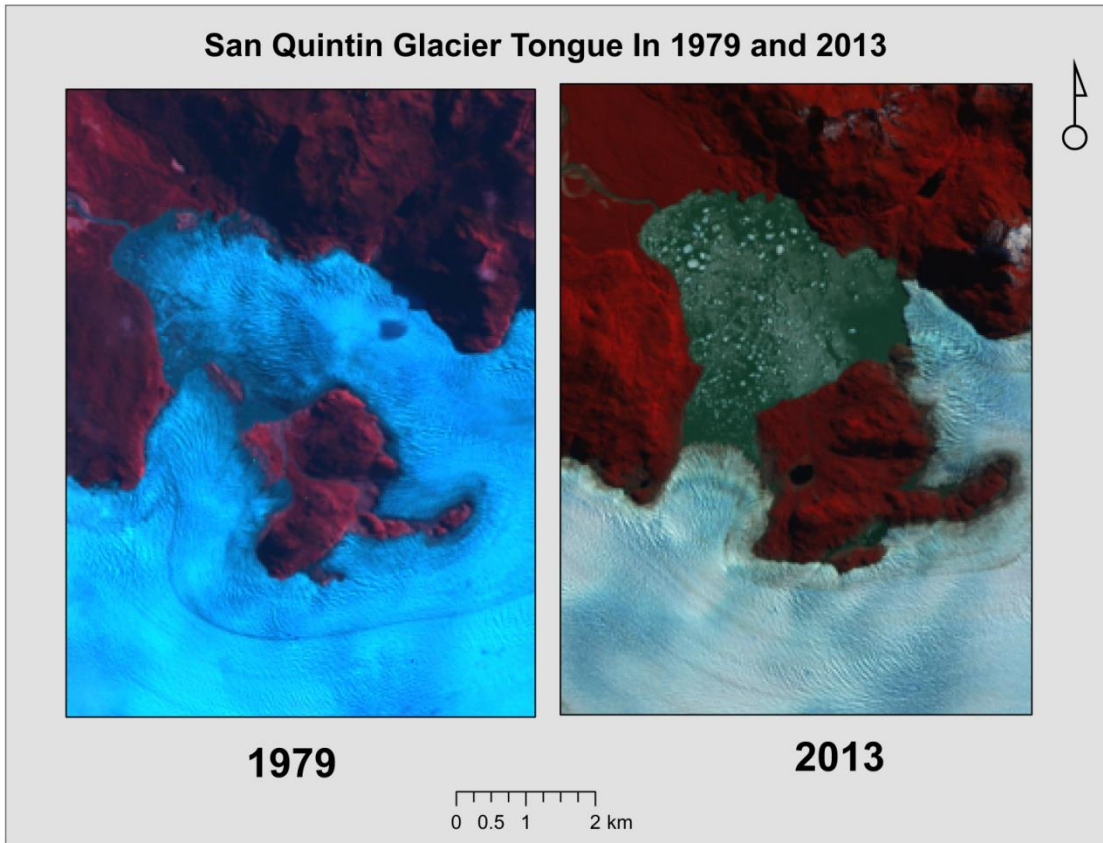
Figure 4.2   San Quintin glacier retreats to form a new lake in 2013.
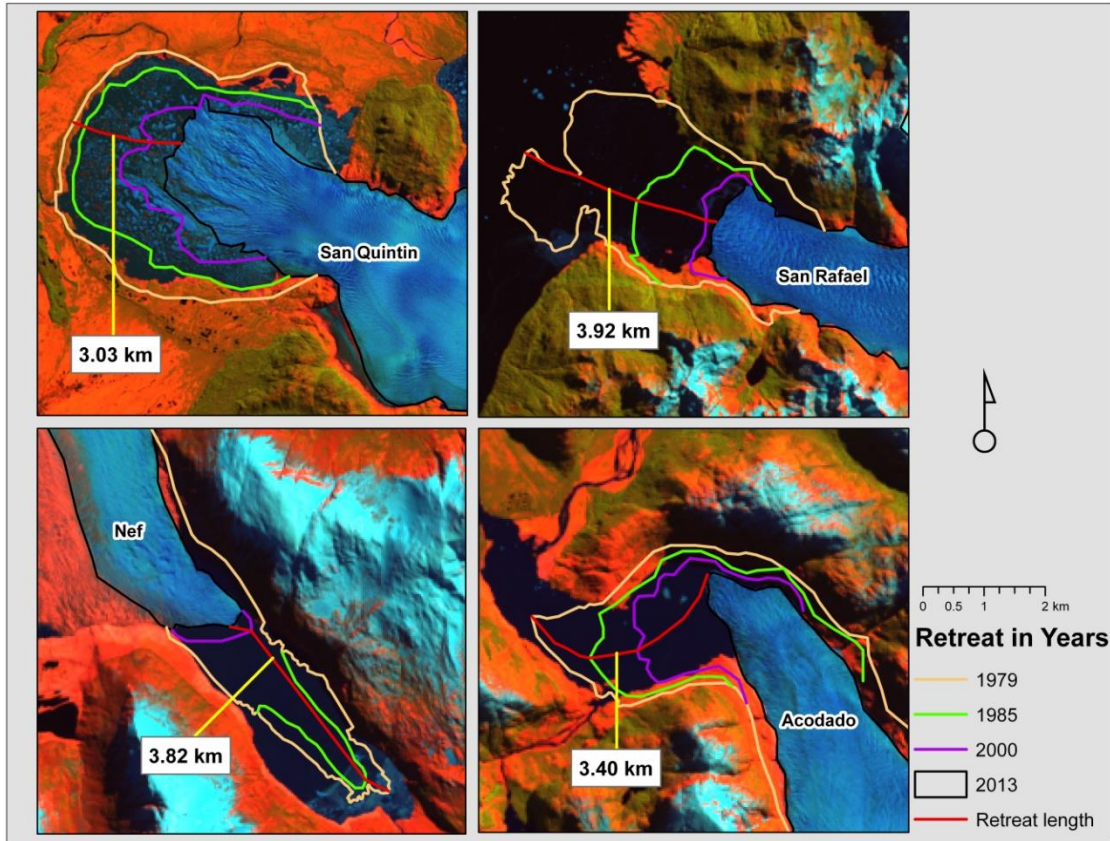
Figure 4.3   Retreat in San Quintin, San Rafael, Nef and Acodado glacier.
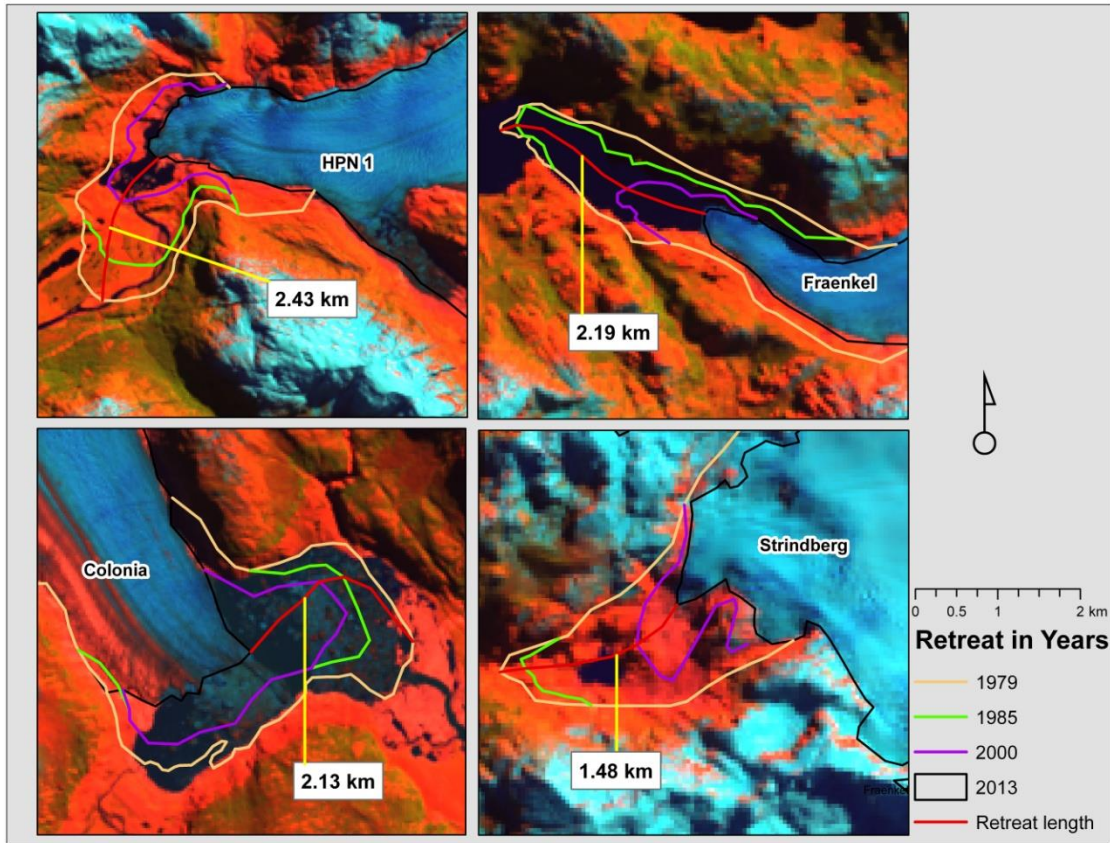
Figure 4.4   Retreat in HPN-1, Fraenkel, Colonia and Strindberg glacier.
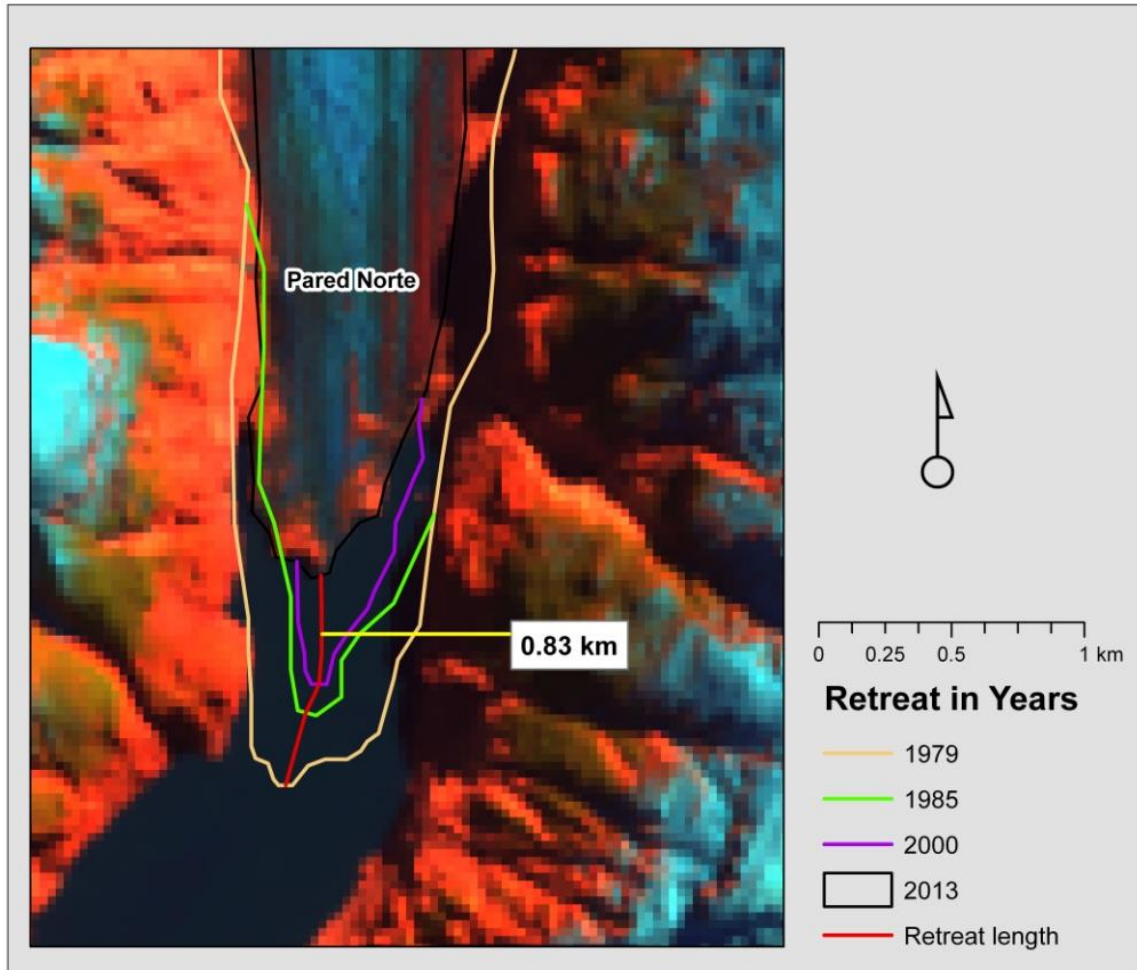
Figure 4.5   Retreat in Pared Norte glacier

Table 4.5   Retreat of glaciers in the NPI

Glacier	Retreat (km)
San Quintin	4.5
San Rafael	3.92
Nef	3.82
Acodado	3.4
HPN-1	2.43
Fraenkel	2.19
Colonia	2.13
Strindberg	1.48
Pared Norte	0.83

Four new glacial lakes were added between 1979 and 2013. A total of 9 glacier lakes were in 1979 but increased to 13 in 2013. The total area of the glacial lakes increased from 13.49 km^2 to 65.06 km^2 (Table 4.6), representing a percentage increase of 79.3. The expansions of the lakes are shown in Figure 4.6 and Figure 4.7. San Quintin glacial lake experienced the maximum expansion of lake from 5.42 km^2 to 42.37 km^2 (Table 4.7). This is due to the creation of a new glacier lake at the tongue of San Quintin. A similar trend was observed between 1945-2011 by Loriaux and Casassa (2013). They also found this drastic increase in San Quintin Lake compared to other glaciers. Table 4.6 also shows the number of lakes and their total area for the study period.
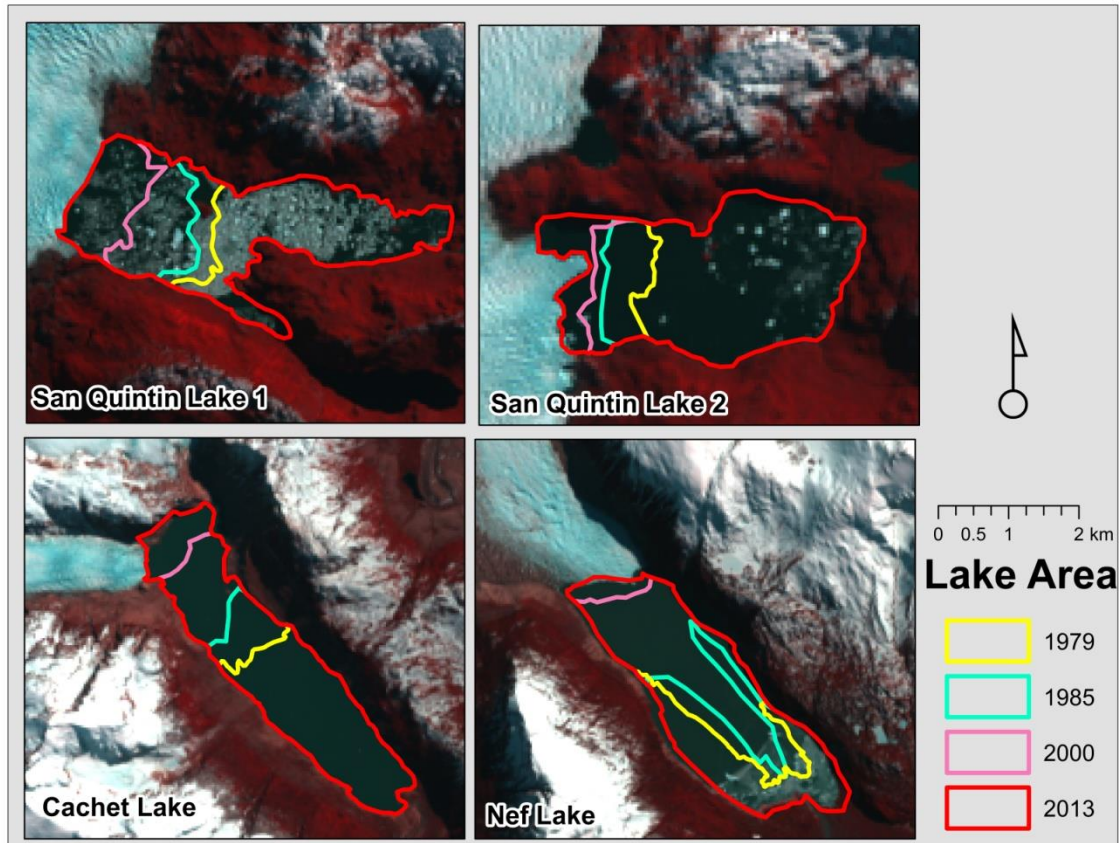
Figure 4.6   Expansion of San Quintin lake 1, San Quintin lake 2, Cachet lake and Nef lake
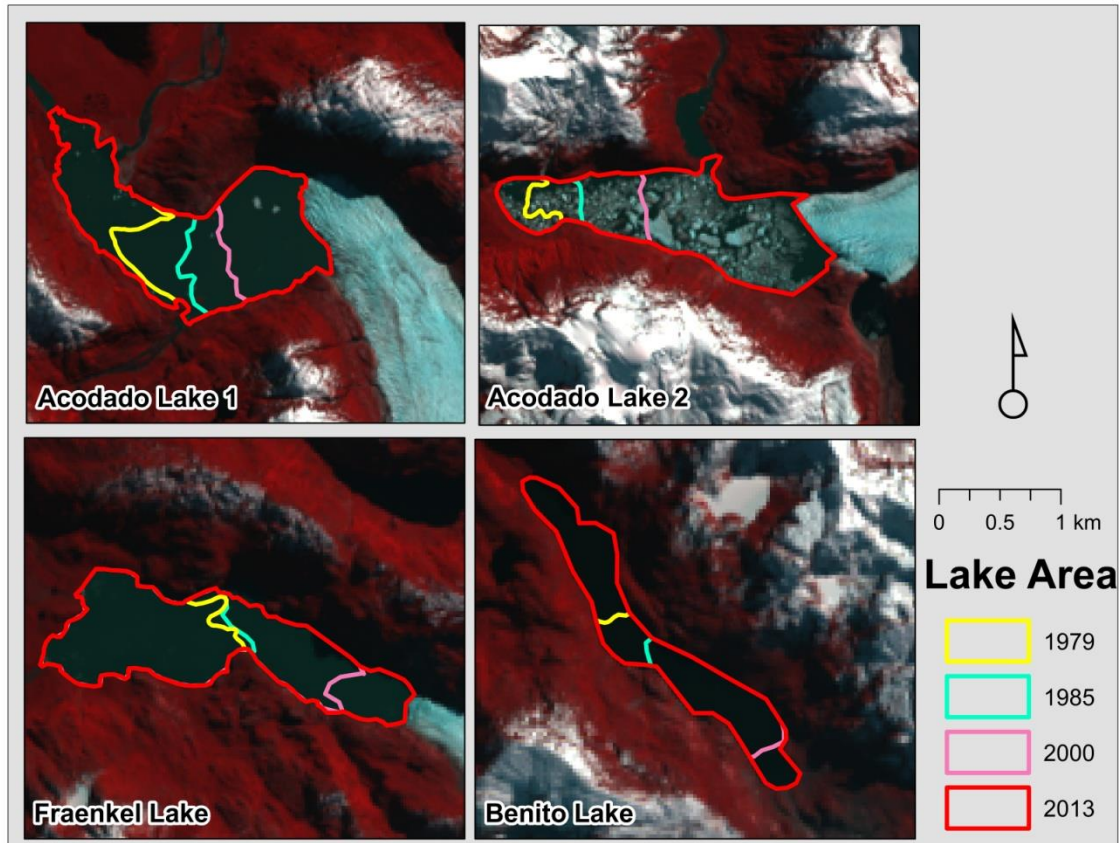
Figure 4.7   Expansion of Acodado lake 1, Acodado lake 2, Fraenkel lake and Benito lake.

Table 4.6   Glacial lakes increase from 1979 to 2013

Year	Number of lakes	Area (sq.km)
1979	9	13.49
1985	10	25.32
2000	11	51.29
2013	13	65.06

Table 4.7   Glacial lakes area for 1979 and 2013

Glacier Lake	1979 Area (sq.km)	2013 Area (sq.km)
San Quintin	5.42	42.37
Fraenkel	1.48	2.41
Benito	0.39	1
Acodado	1.8	9.38
Cachet	2.5	4.3
Nef	1.9	5.6

To test the significance of glacial lake expansion between 1979 and 2013 a paired t-Test was conducted at 95% confidence interval. The result indicated t (5) = -1.49, p = 0.005. Thus, I reject the null hypothesis and accept the alternative hypothesis that glacial lakes have expanded significantly in the study area. Similarly, to test the significance of glacial retreat, a one-sample t-Test was conducted (test value = 0) at 95% confidence interval. The result indicated t (8) = 6.695, p = 0.000. Therefore, I rejected the third null hypothesis and concluded that there is a significant glacial retreat in the study area.

This chapter discussed the results of this study. The mass balance estimates that were given in this study had high uncertainties. This is mainly attributed to heavy snow cover, lack of field GCPs and the high vertical error of 17 m (Falkner, 1995) and high horizontal error of 15 m (NIMA, 1997) in the topographic map that was used as reference. High glacier retreats were recorded in this study and 4 new lakes were formed. This is evidence that glaciers in the NPI are retreating. Chapter IV establishes the conclusions and recommendations for further research.

CHAPTER V

CONCLUSIONS AND RECOMMENDATIONS

There is only one study that has estimated the mass balance of the entire NPI. The

region is neglected for mass balance studies due to the fact that this area is far from the

inhabited residence of the local people, and the poor nature of the weather and terrain

makes it very inaccessible. Therefore, glacier inventory in the WGMS lacks data about

the state of glaciers in the NPI. This makes it very important to study theses glaciers,

since these temperate glaciers respond to climate quickly and can be used to understand

the dynamics of climate change. An early warning system can be developed if the glacial

lakes in this region are studied and monitored to prevent a Glacier Lake Outburst Flood

(GLOF) event.

The study objectives were to;

1. To estimate mass balance of major glaciers in North Patagonia Ice Field

   between 2007 and 2012 using remote sensing techniques.

2. To measure the multi-decadal retreat of the North Patagonian glaciers and

3. to analyze the expansion of glacial lakes using topographic maps and

   Landsat (TM, ETM+ and 8) images between 1979 and 2013.

In this paper, I performed mass balance analysis on 13 glaciers in the NPI using

two ASTER images from 2007 - 2012. Glaciers on the western side of the NPI

experienced more mass loss than glaciers on the eastern side. HPN-4 glacier experienced

the most mass loss with -8.9 $\pm$ 1.96 m.w.e.a.$^{-1}$. Cachet Norte glacier on the western side was almost stable with mass balance of 1.95 ± 1.96 m.w.e.a.$^{-1}$. Nef glacier on the eastern side of the NPI experienced the most mass gain of 9.91 ± 1.96 m.w.e.a.$^{-1}$. Better mass balance rates were observed when the study area was divided in accumulation and ablation zones. Mass balance loss was experienced more in the western glaciers on the ice field. Aniya (1988) explains that, even though the western side of the ice field receives more snow-fall than the eastern side, the eastern side receives more accumulation of snow due to the strong winds that drift snow to the east from the west. Lopez et al. (2008) agree to this phenomenon by adding that snow on the western side melts faster than on the eastern side due to warm air temperature. The fact that this pattern was reflected in the mass balance values in this study shows that the estimates made in this study reflects the nature on the glaciers in the NPI. However, due to high uncertainty in elevation values of the DEMs, mass balance values also had high uncertainties.

Three Landsat images (1985 Landsat 5 TM), 2000 Landsat 7 ETM+, and 2013 Landsat 8) and 1979 1:50,000 topographic maps were used to measure the retreat of the NPI glaciers, and to analyze the expansion of glacial lakes. San Quintin retreated the most by 4.5 km between 1979 and 2013. Some of the glaciers experienced more retreat than others within the same time period. Four new glacial lakes were formed within the time period causing an increase in lake area by 79.3% for the time period. The research results for both mass balance and retreat were not validated with *in-situ* data from the NPI but similar results were observed by Aniya (1988), Aniya (1999), Aniya et al. (1996), Rignot et al. (2003), Rivera et al. (2007), Lopez et al. (2008) and Scaefer et al.

(2013) for glacier thinning and mass balance studies and Lopez et al. (2010), Loriaux and Casassa (2013) and Rivera et al. (2007) for glacier retreat and lakes.

This study recorded a high uncertainty in mass balance, which is because of the heavy snow cover in the ice field. The low quality of the DEM generated is also a factor. This is due to the rugged terrain associated with the NPI and the high vertical random error of 17 m (Falkner, 1995) of the topographic map. The main limitation to this study is the unavailability of GCPs from the NPI. In order to reduce these errors and increase the accuracy of elevation values in the future studies, field work needs to be performed to collect accurate GCPs for a good DEM generation. More detailed mass balance study involving the contribution of climatic factors such as air temperature and precipitation should be performed for future work. This will indicate the climatic factors that influence glacier responses and help to understand the dynamics of climate change in the NPI. However, even with higher uncertainty in the mass balance values (±1.96 m), this study made a significant contribution to the understandings of the spatial and temporal patterns of the glacial changes in the North Patagonian Ice fields of Chile

REFERENCES

Abrams, M. 2000. The Advanced Spaceborne Thermal Emission and Reflection Radiometer (ASTER): data products for the high spatial resolution imager on NASA's Terra platform. *International Journal of Remote sensing*, 21(5): 847-859.

Ambinakudige, S. 2010. A study of the Gangotri glacier retreat in the Himalayas using Landsat satellite images. *International Journal of Geoinformatics,* 6 (3): 7-12.

Ambinakudige, S. 2014. "Glaciers." In *Oxford Bibliographies in Geography*. Ed. Barney Warf. New York: Oxford University Press.

Ambinakudige, S., and K. Joshi. 2013. An Analysis of Fedchenko and surrounding glaciers mass balance 2004-2009, Tajikistan. Davos Atmosphere and Cryosphere Assembly. Davos, Switzerland. July 8-12, 2013.

Ames, A. 1998. A documentation of glacier tongue variations and lake development in the Cordillera Blanca, Peru. *Zeitschrift für Gletscherkunde und Glazialgeologie,* 34: 1-36.

Aniya, M., 1988. Glacier inventory for the Northern Patagonia Ice field, Chile, and variations 1944/45 to 1985/86. *Arctic and Alpine Research,* 20 (2): 179-187.

Aniya, M., 1992. Glacier variation in the Northern Patagonia Ice field, Chile, between 1985/86 and 1990/91. *Bulletin of Glaciological Research,* 10: 83-90.

Aniya, M., 1999. Recent glacier variations of the Hielos Patagonicos, South America, and their contribution to sea-level change. *Artic, Antarctic and Alpine Research,* 31 (2): 165-173.

Aniya, M., 2007. Glacier variations of Hielo Patagonico Norte, Chile, for 1944/45-2004/ 05. *Bulletin of Glaciological Research,* 24: 59-70.

Aniya, M., and H. Enomoto. 1986. Glacier variations and their causes in the Northern Patagonia Ice field, Chile, since 1944. *Arctic and Alpine Research,* 307-316.

Aniya, M., H. Sato, R. Naruse, P. Skvarca, and G. Casassa. 1996. The use of satellite and airborne imagery to inventory outlet glaciers of the Southern Patagonia Ice field, South America. *Photogrammetric Engineering and Remote Sensing*, 62 (12): 1361-1369.

Barry, R. G. 2006. The status of research on glaciers and global glacier recession: a review. *Progress in Physical Geography*, 30(3): 285-306.

Berthier E., Y. Arnaud, K. Rajesh, A. Sarfaraz, P. Wagnon, and P. Chevallier. 2007. Remote sensing estimates of glacier mass balances in the Himachal Pradesh (Western Himalaya, India). *Remote Sensing Environ,* 108(3): 327-338.

Bolch, T., J. Peters, A.Yegorov, B. Pradhan, M. Buchroithner, and V. Blagoveshchensky. 2012. Identification of Potentially Dangerous Glacial Lakes in the Northern Tian Shan. In *Terrigenous Mass Movements,* 369-398. Springer Berlin Heidelberg.

Bolch, T., T. Pieczonka, and D. I. Benn. 2011. Multi-decadal mass loss of glaciers in the Everest area (Nepal Himalaya) derived from stereo imagery. *The Cryosphere*, 5(2): 349-358.

Bolch, T., M. Buchroithner, T. Pieczonka, and A. Kunert. 2008. Planimetric and volumetric glacier changes in Khumbu Himalaya since 1962 using Corona, Landsat TM and ASTER data. *Journal of Glaciology,* 54: 592-600.

Berthier, E., Y Arnaud, R. Kumar, S. Ahmad, P. Wangnon, and P. Chevallier. 2007. Remote Sensing Estimates of Glacier Mass Balances in the Himachal Pradesh (Western Himalaya, India). *Remote Sensing of Environment,* 108: 327-338.

Braithwaite, R. 2002. Glacier mass balance: the first 50 years of international monitoring. *Progress in Physical Geography,* 26 (1): 76-95.

Braithwaite, R. J., and S. C. B. Raper. 2010. Estimating equilibrium-line altitude (ELA) from glacier inventory data. *Annals of Glaciology*, 50(53): 127-132.

Carrasco, J., G. Casassa, and A. Rivera. 2002. Meteorological and climatological aspects of the Southern Patagonia Icefield. In: Casassa, G., Sepulveda, F., Sinclair, R. (Eds.), The Patagonian Icefields. A unique Natural Laboratory for Environmental and Climate Change Studies. *Kluwer Academic/Plenum Publishers New York*, 29-65.

Casassa, G., J. Wendt, A. Wendt, P. López, T. Schuler, H. Maas, J. Carrasco, and A. Rivera. "Outburst floods of glacial lakes in Patagonia: is there an increasing trend?." In *EGU General Assembly Conference Abstracts*, 12: 12821-2010.

Casassa, G., W. Haeberli, G. Jones, G. Kaser, P. Ribstein, A. Rivera, and C. Schneider. 2007. Current status of Andean glaciers. *Global and Planetary Change*, 59(1): 1-9.

Casey, K., A. Kaab, and D. Benn. 2012. Geochemical characterization of supraglacial debris via in situ and optical remote sensing methods: a case study in Khumbu Himalaya, Nepal. *The Cryosphere,* 6: 85-100.

Carey, M. 2005. Living and dying with glaciers: people's historical vulnerability to avalanches and outburst floods in Peru. *Global and planetary change*, 47(2): 122-134.

Clague, J., and S. Evans. 2000. A review of catastrophic drainage of moraine-dammed lakes in British Columbia. *Quaternary Science Reviews,* 19: 1763-1783.

Cook, A. J., T. Murray, A. Luckman, D. E. Vaughan, and N. E. Barrand. 2012. A new 100-m Digital Elevation Model of the Antarctic Peninsula derived from ASTER Global DEM: methods and accuracy assessment. *Earth System Science,* 4(1): 129-142.

Dyurgerov, M., and M. Meier. 1997. Mass balance of mountain and sub polar glaciers: a new assessment for 1961–1990. *Alpine Research,* 29: 379-391.

Enomoto, H., C. Nakajima. 1985. Recent climate-fluctuations in Patagonia. In: Nakajima, C. (Ed.), Glaciological studies in Patagonia Northern Icefield 1983–1984. Data Center for Glacier Research. *Japanese Society of Snow and Ice, Nagoya Japan,* 7-14.

Escobar, F., F. Vidal, C. Garin. 1992. Water balance in the Patagonia Icefield. In: Naruse, R. (Ed.), Glaciological Researches in Patagonia. *Japanese Society of Snow and Ice,* 109-119.

Falkner, E., 1995. Aerial Mapping. Methods and Applications. *CRC Press Inc, USA*. 322

Fischer, A. 2011. Comparison of direct and geodetic mass balances on a multi-annual time scale. *The Cryosphere*, 5(1): 107-124.

Fischer, L., A. Kääb, C. Huggel, and J. Noetzli. 2006. Geology, glacier retreat and permafrost degradation as controlling factors of slope instabilities in a high-mountain rock wall: the Monte Rosa east face. *Natural Hazards & Earth System Sciences*, 6(5).

Fujiyoshi, Y., H. Kondo, J. Inoue, and T. Yamada. 1987. Characteristics of precipitation and vertical structure of air temperature in the northern Patagonia. *Bulletin of Glacier Research,* 4: 15-23.

Garreaud, R., M. Vuille, R. Campagnucci, and J. Marengo. 2007. Present-day South American climate. *Palaeogeography, Palaeoclimatology, Palaeoecology*.doi:10.1016/ j.palaeo.2007.10.032.

Gardelle, J., E. Berthier, and Y. Arnaud. 2012. Slight mass gain of Karakoram glaciers in the early twenty-first century. *Nature geoscience*, 5(5): 322-325.

Harrison, S., V. Winchester. 1998. Historical fluctuations of the Gualas and Reicher Glaciers, North Patagonian Icefield, Chile. *The Holocene,* 8(4): 481-485.

Harrison, S., N. Glasser, V. Winchester, E. Haresign, C. Warren, and K. Jansson. 2006. A glacial lake outburst flood associated with recent mountain glacier retreat, Patagonian Andes. *The Holocene*, 16(4): 611-620.

Hirano, A., W. Roy, and H. Lang. 2003. Mapping from ASTER Stereo Image Data: DEM Validation and Accuracy Assessment. *ISPRS Journal of Photogrammetry and Remote Sensing,* 57(5): 356-370.

Hoffmann, D., and D. Weggenmann. 2013. Climate Change Induced Glacier Retreat and Risk Management: Glacial Lake Outburst Floods (GLOFs) in the Apolobamba Mountain Range, Bolivia. In *Climate change and disaster risk management*, 71-87. Springer Berlin Heidelberg.

Houghton J. T., Y. Ding, D. J. Griggs, M . Noguer, P. J. Van Der Hinden, X. Dai, K. Maskell, C. A. Johnson. 2001. Climate Change 2001: *The Scientific Basis. Cambridge University Press: Cambridge*.

Howat, Ian M., and A. Eddy. 2011. Multi-decadal retreat of Greenland's marine-terminating glaciers. *Journal of Glaciology*, 57(203): 389-396.

Hubbard, B., and N. Glasser. 2005. *Field Techniques in Glaciology and Glacial Geomorphology: Glacier Mass Balance and Motion*. John Wiley & Sons, Ltd. Chichester, England: 179-216.

Huggel, C., A. Kaab, W. Haeberli, P. Teysseire, and F. Paul. 2002. Remote sensing based assessment of hazards from glacier lake outbursts: a case study in the Swiss Alps. *Canadian Geotechnical Journal,* 39: 316-330.

Huss, M., and A. Bauder. 2009.. 20th-century climate change inferred from four long-term point observations of seasonal mass balance. *Annals of Glaciology,* 50(50): 207-214.

IPCC, 2007: Climate Change 2007: The Physical Science Basis. Contribution of Working Group I to the Fourth Assessment Report of the Intergovernmental Panel on Climate Change [Solomon, S., D. Qin, M. Manning, Z. Chen, M. Marquis, K.B. Averyt, M.Tignor and H.L. Miller (eds.)]. *Cambridge University Press, Cambridge, United Kingdom and New York, NY, USA*.

IPCC, 2013: Summary for Policymakers. In: Climate Change 2013: The Physical Science Basis. Contribution of Working Group I to the Fifth Assessment Report of the Intergovernmental Panel on Climate Change [Stocker, T.F., D. Qin, G.-K. Plattner, M. Tignor, S. K. Allen, J. Boschung, A. Nauels, Y. Xia, V. Bex and P.M. Midgley (eds.)]. *Cambridge University Press, Cambridge, United Kingdom and New York, NY, USA*.

Kaab, A. 2008. Glacier volume changes using ASTER satellite stereo and ICESat GLAS laser altimetry. A test study on Edgeøya, Eastern Svalbard. *Geoscience and Remote Sensing, IEEE Transactions on*, 46(10): 2823-2830.

Kääb, A., J. M. Reynolds, and W. Haeberli. Glacier and permafrost hazards in high mountains. In *Global change and mountain regions* 225-234. Springer Netherlands, 2005.

Kargel, J., M. Abrams, M. Bishop, A. Bush, and G. Hamilton. 2005. Multispectral imaging contributions to global land ice measurements from space. *Remote Sensing of Environment,* 99 (1-2): 187-219.

Kaser, G., A. Fountain, and P. Jansson. 2003. *A manual for monitoring the mass balance of mountain glaciers*. Technical Documents in Hydrology, 59:106. UNESCO, Paris.

La Frenierre, J. The Utility of Laser Scanning for Monitoring Debris-Covered Glaciers and Assessing GLOF Hazard in the Khumbu Himalaya, Nepal.

Liu, K., C. A. Reese, & L. G. Thompson. 2005. Ice-core pollen record of climatic changes in the central Andes during the last 400 yr. *Quat. Res*., 64: 272-278.

Lliboutry, L., 1998. Glaciers of Wet Andes. In: Williams, M., J. Ferrigno (Eds.), Satellite image atlas of glaciers of the world. *U.S. Government Printing Office, Washington, D.C*, I109–I206.

López-Moreno, J. I., S. Fontaneda, J. Bazo, J. Revuelto, C. Azorin-Molina, B. Valero-Garcés, E. Morán-Tejeda, S. M. Vicente-Serrano, R. Zubieta, and J. Alejo-Cochachín. 2014. Recent glacier retreat and climate trends in Cordillera Huaytapallana, Peru. *Global and Planetary Change*, 112: 1-11.

López, P., and G. Casassa. 2011. Recent acceleration of ice loss in the Northern Patagonia Icefield based on an updated decennial evolution. *The Cryosphere Discuss,* 5(6): 3323-3381.

Lopez, P., P. Chevallier, V. Favier, B. Pouyaud, F. Ordenes, and J. Oerlemans. 2010. A regional view of fluctuations in glacier length in southern South America. *Global and Planetary Change*, 71(1): 85-108.

Lopez, P., P. Sirguey, Y. Arnaud, B. Pouyaud, and P. Chevallier. 2008 Snow cover monitoring in the Northern Patagonia Icefield using MODIS satellite images (2000–2006). *Global and Planetary Change*, 61(3): 103-116.

Loriaux, T., and G. Casassa. 2013. Evolution of glacial lakes from the Northern Patagonia Icefield and terrestrial water storage in a sea-level rise context. *Global and Planetary Change*, 102: 33-40.

Matsuoka, K., and R. Naruse. Mass balance features derived from a firn core at Hielo Patagonico Norte, South America. *Arctic, Antarctic, and Alpine Research*, 31(4): 333-340.

Mukherjee, S., P. K. Joshi, S. Mukherjee, A. Ghosh, R. D. Garg, and A. Mukhopadhyay. 2013. Evaluation of vertical accuracy of open source Digital Elevation Model (DEM). *International Journal of Applied Earth Observation and Geoinformation*, 21: 205-217.

Muukkonen, P., and J. Heiskanen. 2007. Biomass estimation over a large area based on standwise forest inventory data and ASTER and MODIS satellite data: A possibility to verify carbon inventories. *Remote Sensing of Environment*, 107(4): 617-624.

NIMA (National Imagery and Mapping Agency), 1997. Department of Defense World Geodetic System 1984: its definition and relationships with local geodetic systems. NIMA TR8350.2 Third Edition 4 July 1997. *National Imagery and Mapping Agency*, Bethesda, MD.

Nishida, K., K. Satow, M. Aniya, G. Casassa, and T. Kadota. 1995. Thickness change and flow of Tyndall Glacier, Patagonia. *Bulletin of Glacier Research,* 13: 29-34.

Nuth, C., and A. Kääb. 2011. Co-registration and bias corrections of satellite elevation data sets for quantifying glacier thickness change. *The Cryosphere*, 5(1): 271-290.

Paterson, W. 1994. *The Physics of Glaciers*, (3rd ed.). Pergamon, Oxford.

Pellicciotti, F., S. Ragettli, M. Carenzo, and J. McPhee. 2013. Changes of glaciers in the Andes of Chile and priorities for future work. *Science of The Total Environment*.

Pieczonka, T., T. Bolch, W. Junfeng, and L. Shiyin. 2013. Heterogeneous mass loss of glaciers in the Aksu-Tarim Catchment (Central Tien Shan) revealed by 1976 KH-9 Hexagon and 2009 SPOT-5 stereo imagery. *Remote Sensing of Environment*, 130: 233-244.

Racoviteanu, A., Y. Arnaud, M. Williams, and J. Ordonez. 2008. Decadal changes in glacier parameters in the Cordillera Blanca, Peru, derived from remote sensing. *Journal of Glaciology,* 54(186): 499-510.

Raup, B., A. Racoviteanu, S. J. S. Khalsa, . Helm, R. Armstrong, and Y. Arnaud. 2007. The GLIMS geospatial glacier database: A new tool for studying glacier change. *Global and Planetary Change,* 56(1): 101-110.

Reynolds, J. M. 1992. The identification and mitigation of glacier-related hazards: examples from the Cordillera Blanca, Peru. *In Geohazards,* 143-157. Springer Netherlands.

Richardson, S., and J. Reynolds. 2000. An overview of glacial hazards in the Himalayas. *Quaternary International,* 65-66: 31-47.

Rignot, E., A. Rivera, and G. Casassa. 2003. Contribution of the Patagonia Icefields of South America to sea level rise. *Science,* 302(5644): 434-437.

Rivera, A., G. Casassa, C. Acuña, and H. Lange. 2000. Variaciones recientes de glaciares en Chile. *Investigaciones Geográficas* 34: 25-52.

Rivera, A., T. Benham, G. Casassa, J. Bamber and J. Dowdeswell. 2007. Ice elevation and areal changes of glaciers from the Northern Patagonia icefield, Chile. *Global and Planetary Change* 59 (1): 126-137.

Rott, H., W. Rack, P. Skvarca, and H. De Angelis. 2002. Northern Larsen Ice Shelf, Antarctica: further retreat after collapse, *Annals of Glaciology,* 34: 277-282.

Schaefer, M., H. Machguth, M. Falvey, and G. Casassa. 2013. Modeling past and future surface mass balance of the Northern Patagonia Icefield. *Journal of Geophysical Research: Earth Surface,* 118(2): 571-588.

Schaffhauser, A., M. Adams, R. Fromm, P. Jörg, G. Luzi, L. Noferini, and R. Sailer. 2008. Remote sensing based retrieval of snow cover properties. *Cold Regions Science and Technology,* 54(3): 164-175.

Wang, J., K. Di, and R. Li. Evaluation and improvement of geopositioning accuracy of IKONOS stereo imagery. *Journal of surveying engineering,* 131(2): 35-42.

Warren, C., and M. Aniya. 1999. The calving glaciers of southern South America. *Global and Planetary Change,* 22(1): 59-77.

Warren, C. R., and D. E. Sugden. 1993. The Patagonian Icefields: a glaciological review. *Arctic and Alpine Research,* 25(4): 316-331.

Willis, M. J., A. K. Melkonian, M. E. Pritchard, and J. M. Ramage. 2012 Ice loss rates at the Northern Patagonian Icefield derived using a decade of satellite remote sensing. *Remote Sensing of Environment,* 117: 184-198.

Winchester, V., S. Harrison. 1996. Recent oscillations of the San Quintín and San Rafael glaciers, Patagonian Chile. *Geografiska Annaler,* 78a(1): 35–49.

Wu, S. S., Z. J. Yao, H. Q. Huang, Z. F. Liu, and G. H. Liu. 2012. Responses of glaciers and glacial lakes to climate variation between 1975 and 2005 in the Rongxer basin of Tibet, China and Nepal. *Regional Environmental Change,* 12(4): 887-898.

Yamada, T. 1987. Glaciological characteristics revealed by 37.6-m deep core drilled at the accumulation area of San Rafael Glacier, the Northern Patagonia Icefield. *Bulletin of glacier research*, 4: 59-67.

Yamanda, T., and C. Sharma. 1993. Glacier Lakes Outburst Floods in the Nepal Himalaya. *Snow and Glacier Hydrology, proceedings of the Kathmandu Symposium*, November 1992. IAHS 218: 319-330.

Yamaguchi, Y., A. B. Kahle, H. Tsu, T. Kawakami, and M. Pniel. 1998. Overview of Advanced Spaceborne Thermal Emission and Reflection Radiometer (ASTER). *IEEE Transactions on Geoscience and Remote Sensing,* 36: 1062 – 1071. Zemp, M., M. Hoelzle, and W. Haeberli. 2009. Six decades of glacier mass-

balance observations: a review of the worldwide monitoring network. *Annals of*

Glaciology, 50(50): 101-111.

APPENDIX A

T-TEST RESULTS FOR NON-GLACIALTED AND GLACIATED REGION FOR THE

STUDY PERIOD 2007-2012

T-Test on Non-glaciated region, 2007-2012

Paired Samples Statistics

	Mean	N	Std. Deviation	Std. Error Mean
Pair 1 Year 2012	568.5736	192518	420.8320	0.9591
Year 2007	572.2198	192518	419.7773	0.9567

Paired Samples Correlations

	N	Correlation	Sig.
Pair 1 Year 2012 and Year 2007	192518	0.990	0.000

Paired Samples Test

	Paired Differences							Sig. (2-tailed)
				95% Confidence Interval of the Difference				
	Mean	Std. Deviation	Std. Error Mean	Lower	Upper	t	df	
Pair 1 Year 2012 - Year 2007	-3.6462	57.8058	0.1317	-3.9044	-3.3880	-27.6763	192517	0.00

T-Test on glaciated region, 2007-2012

Name = Acodado

Paired Samples Statistics[a]

	Mean	N	Std. Deviation	Std. Error Mean
Pair 1	2012	1486.3918	72787	397.1995	1.4722
	2007	1535.6819	72787	378.9809	1.4047

a. Name = Acodado

Paired Samples Correlations[a]

		N	Correlation	Sig.
Pair 1	2012 and 2007	72787	.996	.000

a. Name = Acodado

Paired Samples Test[a]

| | Paired Differences | | | | | | | | |
| | | | | 95% Confidence Interval of the Difference | | | | |
	Mean	Std. Deviation	Std. Error Mean	Lower	Upper	t	df	Sig. (2-tailed)
Pair 1 2007 - 2012	-49.2900	38.3509	0.1421	-49.5686	-49.0113	-346.7443	72786	.000

Name = Arco

Paired Samples Statistics[a]

		Mean	N	Std. Deviation	Std. Error Mean
Pair 1	2012	2163.1723	3585	248.7689	4.1548
	2007	2238.3495	3585	237.8494	3.9724

a. Name = Arco

Paired Samples Correlations[a]

		N	Correlation	Sig.
Pair 1	2012 and 2007	3585	.978	0.000

Paired Samples Test[a]

		Paired Differences					t	df	Sig. (2-tailed)
					95% Confidence Interval of the Difference				
		Mean	Std. Deviation	Std. Error Mean	Lower	Upper			
Pair 1	2007 - 2012	-75.1771	52.3631	0.8745	-2.80285	-73.4624	-85.9616	3584	.000

Name = Benito

Paired Samples Statistics[a]

		Mean	N	Std. Deviation	Std. Error Mean
Pair 1	2012	1039.9181	62671	524.2130	2.0939
	2007	1039.2048	62671	514.0823	2.0535

a. Name = Benito

Paired Samples Correlations^a

		N	Correlation	Sig.
Pair 1	2012 and 2007	62671	.998	0.000

a. Name = Benito

Paired Samples Test^a

		Paired Differences							
					95% Confidence Interval of the Difference				
		Mean	Std. Deviation	Std. Error Mean	Lower	Upper	t	df	Sig. (2-tailed)
Pair 1	2007 - 2012	0.7133	30.6473	0.1224	0.4733	0.9532	5.8266	62670	0.000

a. Name = Benito

Name = Cachet

Paired Samples Statistics^a

		Mean	N	Std. Deviation	Std. Error Mean
Pair 1	2012	1522.0289	14314	313.2083	2.6178
	2007	1481.7334	14314	323.3038	2.7022

a. Name = Cache

78

Paired Samples Correlations[a]

	N	Correlation	Sig.
Pair 1 2012 and 2007	14314	.990	0.000

a. Name = Cachet

Paired Samples Test[a]

	Paired Differences					t	df	Sig. (2-tailed)
	Mean	Std. Deviation	Std. Error Mean	95% Confidence Interval of the Difference				
				Lower	Upper			
Pair 1 2007 - 2012	40.2955	46.7175	0.3904	39.5301	41.0609	103.1948	14313	.000

a. Name = Cachet

Name = Cachet Norte

Paired Samples Statistics[a]

	Mean	N	Std. Deviation	Std. Error Mean
Pair 1 2012	1262.1572	3365	342.8191	5.9097
2007	1223.3218	3365	365.4886	6.3005

a. Name = Cachet Norte

Paired Samples Correlations[a]

	N	Correlation	Sig.
Pair 1 2012 and 2007	3365	.992	0.000

a. Name = Cachet Norte

Paired Samples Test[a]

	Paired Differences							
				95% Confidence Interval of the Difference				
	Mean	Std. Deviation	Std. Error Mean	Lower	Upper	t	df	Sig. (2-tailed)
Pair 1 2007 - 2012	38.8353	50.2709	0.8666	37.1362	40.5345	44.8129	3364	.000

a. Name = Cachet Norte

80

Name = Colonia

Paired Samples Statistics[a]

		Mean	N	Std. Deviation	Std. Error Mean
Pair 1	2012	1604.3854	91099	499.0397	1.6534
	2007	1620.6977	91099	509.3523	1.6875

a. Name = Colonia

Paired Samples Correlations[a]

	N	Correlation	Sig.
Pair 1 2012 and 2007	91099	.997	0.000

a. Name = Colonia

81

Paired Samples Test[a]

	Paired Differences					t	df	Sig. (2-tailed)
	Mean	Std. Deviation	Std. Error Mean	95% Confidence Interval of the Difference				
				Lower	Upper			
Pair 1 2007 - 2012	-16.3122	52.9638	0.1754	-16.6562	-15.9683	-92.9589	91098	.000

a. Name = Colonia

Name = Fraenkel

Paired Samples Statistics[a]

	Mean	N	Std. Deviation	Std. Error Mean
Pair 1 2012	1242.2083	12632	512.5245	4.5601
2007	1193.3346	12632	494.5642	4.4003

a. Name = Fraenkel

Paired Samples Correlations[a]

	N	Correlation	Sig.
Pair 1 2012 and 2007	12632	.999	0.000

a. Name = Fraenkel

Paired Samples Test[a]

	Paired Differences					t	df	Sig. (2-tailed)
	Mean	Std. Deviation	Std. Error Mean	95% Confidence Interval of the Difference				
				Lower	Upper			
Pair 1 2007 - 2012	15.31340	99.15385	2.85638	9.70937	20.91744	5.361	1204	.000

Name = HPN 1

Paired Samples Statistics[a]

	Mean	N	Std. Deviation	Std. Error Mean
Pair 1 2012	935.3515	94008	363.1921	1.1845
2007	977.7761	94008	343.4626	1.1202

a. Name = HPN 1

Paired Samples Correlations[a]

	N	Correlation	Sig.
Pair 1 2012 and 2007	94008	.995	0.000

a. Name = HPN 1

Paired Samples Test[a]

	Paired Differences					t	df	Sig. (2-tailed)
				95% Confidence Interval of the Difference				
	Mean	Std. Deviation	Std. Error Mean	Lower	Upper			
Pair 1 2007 - 2012	-42.4245	39.2143	0.1278	-42.6752	-42.1738	-331.7069	94007	0.000

a. Name = HPN 1

Name = HPN 4

Paired Samples Statistics[a]

	Mean	N	Std. Deviation	Std. Error Mean
Pair 1 2012	1452.2294	69684	410.3762	1.5545
2007	1543.4872	69684	402.2190	1.5236

a. Name = HPN 4

Paired Samples Correlations[a]

	N	Correlation	Sig.
Pair 1 2012 and 2007	69684	.997	0.000

a. Name = HPN 4

84

Paired Samples Test[a]

	Paired Differences					t	df	Sig. (2-tailed)
	Mean	Std. Deviation	Std. Error Mean	95% Confidence Interval of the Difference				
				Lower	Upper			
Pair 1 2007 - 2012	-91.2578	33.7300	0.1277	-91.5082	-91.0073	-714.199	69683	.000

Name = Nef

Paired Samples Statistics[a]

		Mean	N	Std. Deviation	Std. Error Mean
Pair 1	2012	1343.1430	23145	473.9953	3.1156
	2007	1248.9152	23145	485.6919	3.1925

a. Name = Nef

Paired Samples Correlations[a]

		N	Correlation	Sig.
Pair 1	2012 and 2007	23145	.965	0.000

a. Name = Nef

85

Paired Samples Test[a]

		Paired Differences							
					95% Confidence Interval of the Difference				Sig. (2-tailed)
		Mean	Std. Deviation	Std. Error Mean	Lower	Upper	t	df	
Pair 1	2007 - 2012	94.2278	49.8650	0.3277	93.5854	94.8703	287.4824	23144	.000

a. Name = Nef

Name = San Quintin

Paired Samples Statistics[a]

		Mean	N	Std. Deviation	Std. Error Mean
Pair 1	2012	1300.4421	152586	488.3055	1.2500
	2007	1242.0903	152586	464.5478	1.1892

a. Name = San Quintin

Paired Samples Correlations[a]

		N	Correlation	Sig.
Pair 1	2012 and 2007	152586	.996	.000

a. Name = San Quintin

86

Paired Samples Test[a]

	Paired Differences					t	df	Sig. (2-tailed)
				95% Confidence Interval of the Difference				
	Mean	Std. Deviation	Std. Error Mean	Lower	Upper			
Pair 1	2007 - 2012	58.3517	49.0020	0.1254	58.1059	58.5976	465.1549	152585	.000

a. Name = San Quintin

Name = Strinberg

Paired Samples Statistics[a]

	Mean	N	Std. Deviation	Std. Error Mean
Pair 1	2012	1139.3737	7596	207.4632	2.3803
	2007	1080.8042	7596	200.5479	2.3010

a. Name = Strinberg

87

Paired Samples Correlations[a]

	N	Correlation	Sig.
Pair 1 2012 and 2007	7596	.984	.000

a. Name = Strinberg

Paired Samples Test[a]

	Paired Differences						t	df	Sig. (2-tailed)
				Std. Error Mean	95% Confidence Interval of the Difference				
	Mean	Std. Deviation			Lower	Upper			
Pair 1 2007 - 2012	58.5695	36.7115		0.4212	57.7438	59.3952	139.0469	7595	.000

a. Name = Strinberg

88

Name = U5

Paired Samples Statistics[a]

		Mean	N	Std. Deviation	Std. Error Mean
Pair 1	2012	1315.4896	1977	373.6883	8.4043
	2007	1281.0591	1977	417.4731	9.3891

a. Name = U5

Paired Samples Correlations[a]

		N	Correlation	Sig.
Pair 1	2012 and 2007	1977	.991	0.000

a. Name = U5

Paired Samples Test[a]

	Paired Differences							
				95% Confidence Interval of the Difference				Sig. (2-tailed)
	Mean	Std. Deviation	Std. Error Mean	Lower	Upper	t	df	
Pair 1	2007 - 2012	34.4304	69.1444	1.5550	31.3806	37.4802	22.140	1976	.000

APPENDIX B

T-TEST RESULTS FOR GLACIER LAKE EXPANSION AND GLACIER RETREAT

FOR THE STUDY PERIOD 1979-2013

Paired Samples Test for Glacier Lakes Expansion

	Paired Differences					t	df	Sig. (2-tailed)
				95% Confidence Interval of the Difference				
	Mean	Std. Deviation	Std. Error Mean	Lower	Upper			
Pair 1	1979.000000 - 2013.000000	-8.59500	14.12573	5.76681	-23.41905	6.22905	-1.490	5	.005

One-Sample Test for Glacier Retreat

	Test Value = 0					
	t	df	Sig. (2-tailed)	Mean Difference	95% Confidence Interval of the Difference	
					Lower	Upper
Retreat (km)	6.695	8	.000	2.7444	1.799	3.690